NASA CONTRACTOR REPORT

NASA CR-2558

2. 4/4

4.

RELATIONSHIPS BETWEEN MOTION ON ISENTROPIC SURFACES FROM 3-H RAWINSONDE DATA AND RADAR ECHOES

James W. Overall and James R. Scoggins

Prepared by
3. TEXAS A&M UNIVERSITY CENTER FOR APPLIED GEOSCIENCES
College Station, Texas 77843
for George C. Marshall Space Flight Center

5. NATIONAL AERONAUTICS AND SPACE ADMINISTRATION • WASHINGTON, D. C. • MAY 1975

TECHNICAL REPORT S.

1. REPORT NO.	2. GOVERNMENT ACCESSION NO.	3. RECIPIENT'S CATALOG NO.
NASA CR-2558		

4 TITLE AND SUBTITLE	5. REPORT DATE
Relationships Between Motion on Isentropic Surfaces from 3-H Rawinsonde Data and Radar Echoes	MAY 1975
	6. PERFORMING ORGANIZATION CODE M143
7. AUTHOR(S) James W. Overall and James R. Scoggins	8. PERFORMING ORGANIZATION REPORT #
9. PERFORMING ORGANIZATION NAME AND ADDRESS Center for Applied Geosciences, Texas A&M University, College Station, Texas 77843	10. WORK UNIT NO.
	11. CONTRACT OR GRANT NO. NAS8-26751
	13. TYPE OF REPORT & PERIOD COVERED Contractor Report
12. SPONSORING AGENCY NAME AND ADDRESS National Aeronautics and Space Administration, Washington, D. C. 20546	14. SPONSORING AGENCY CODE

15 SUPPLEMENTARY NOTES This work is based on data from AVE II Experiment under Contract NAS8-26751. This work was conducted under the direction of Robert Turner, MSFC, for the Office of Applications, NASA Hq.

16. ABSTRACT

Vertical motion in isentropic surfaces obtained at 3-h intervals from NASA's second Atmospheric Variability (Pilot) Experiment (AVE IIP) conducted on 11 and 12 May 1974 is related to convection indicated by radar echoes. Temporal and spatial changes in vertical motion are shown and demonstrated to be associated with areas of convection.

Vertical motion as large as 22 cm s^{-1} was calculated, and it is shown that vertical motion changes as much as 20 cm s^{-1} in a horizontal distance of 300 km. The rate of change of vertical motion is demonstrated to be as large as 8 cm $s^{-1}h^{-1}$ from data taken at 3-h intervals, while data taken at 12-h intervals the same day displayed a maximum rate of change of 2 cm $s^{-1}h^{-1}$. Radar observations confirmed that the intensity of convection varies as a result of the atmospheric variability as detected by 3-h data but is invisible in data taken at 12-h intervals.

17. KEY WORDS	18. DISTRIBUTION STATEMENT
vertical motion radar atmosphere rawinsonde cloud	UNCLASSIFIED – UNLIMITED CAT 47

19. SECURITY CLASSIF. (of this report)	20. SECURITY CLASSIF. (of this page)	21. NO. OF PAGES	22. PRICE
UNCLASSIFIED	UNCLASSIFIED	67	$4.25

FOREWORD

This report is one of several to be published from research conducted under NASA Contract NAS8-26751 entitled "Relationships Between Vertical Motion on Isentropic Surfaces from 3-H Rawinsonde Data and Radar Echoes". This effort is sponsored by the NASA Office of Applications under the direction of Marshall Space Flight Center's Aerospace Environment Division.. The results presented in this report represent only a portion of the total research effort. Other reports will be published as the research progresses. Data used in the report were taken from the AVE II Experiment conducted during a 24-hour period beginning at 1200 GMT on May 11, 1974, and ending at 1200 GMT on May 12, 1974.

ACKNOWLEDGEMENT

The authors are indebted to the National Aeronautics and Space Administration for providing support for this research under NASA Contract NAS8-26751. We express our thanks to Mr. Robert E. Turner of NASA for his outstanding support in arranging for the AVE IIP experiment and in the reduction of the rawinsonde soundings. Also, special thanks are extended to Miss Cheryl Cunningham, Mrs. Karyl Hayre, and Mrs. Nancy Fucik for typing the text and preparation of the figures.

TABLE OF CONTENTS

TABLE OF CONTENTS (Continued)

LIST OF FIGURES

LIST OF FIGURES (Continued)

LIST OF FIGURES (Continued)

RELATIONSHIPS BETWEEN VERTICAL MOTION ON ISENTROPIC SURFACES FROM 3-H RAWINSONDE DATA AND RADAR ECHOES

by

James W. Overall [1]

and

James R. Scoggins [2]

Center for Applied Geosciences
Texas A&M University

1. INTRODUCTION

Anyone who has viewed a satellite picture of a large area and who has spent a few minutes looking into a cloud-filled sky, realizes there is a wide range of time and space scales for atmospheric phenomena. In order to understand the atmosphere better, a continued effort must be made to describe each scale of motion and to learn the interrelations between scales.

The study of mesoscale systems seems to offer a decided benefit in terms of understanding the atmosphere and improving forecasting skill. Economic constraints and problems associated with data handling and storage are factors that limit the number of observations that can be taken and used. As for upper-air sampling, the standard measurements are spaced roughly 300 km apart horizon-

---

[1] Capt. United States Air Force

[2] Professor of Meteorology and Director, Center for Applied Geosciences, Texas A&M University

tally and at 12-h intervals in time.

Until more data can be taken routinely, carefully-planned data-collection experiments must be carried out in order to learn more about systems that are smaller than the resolution of data now available. The National Aeronautics and Space Administration (NASA) has carried out three Atmospheric Variability Experiments (AVE) and others are planned. The data collected during these experiments were for research purposes and, therefore, have been processed so that they retain the maximum resolution possible.

In this research, an objective analysis that uses potential temperature as the vertical coordinate has been carried out on the second Atmospheric Variability (Pilot) Experiment (AVE IIP) data, collected in the period 1200 GMT 11 May through 1200 GMT 12 May 1974. The purpose of this study is to take advantage of the resolution of these data to further the understanding of vertical motion and its relationship to mesoscale weather systems. Emphasis is placed upon interrelationships between vertical motion, convection, and thunderstorms as detected by radar.

2. BACKGROUND AND STATEMENT OF PROBLEM

a. Statement of problem

Operationally, upper-air measurements are taken at 12-h intervals even though it is obvious that major weather changes take place in shorter intervals. Much has been written about systems that are not detectable with 12-h data but produce much of what is referred to as intermittent weather conditions. The initiation and maintenance of these mesoscale systems are not well understood, but it is known that they produce much of the observed clouds and precipitation. Thunderstorms and other convective clouds form a large part of such systems.

Convective systems such as thunderstorms may form, go through their life cycle, and dissipate without leaving any trace of their existence during the period of 12 h separating usual sounding times. Yet, it is known that these systems have an enormous influence on local weather such as precipitation, temperature, and cloudiness as well as the wind field in their vicinity and heat balance and electrical properties of the atmosphere. Moreover, it is known that large-scale vertical motion is associated with the formation of these convective systems, but it is not known how the vertical motion field varies in magnitude with time during the 12 h between normal sounding times.

b. Previous studies

A limiting factor in the understanding of subsynoptic-scale weather systems is a lack of resolution in available data. Over the years, several programs have been undertaken to collect data that would contain measurements of mesoscale systems.

Elliot and Hovind (1965) studied subsynoptic variations in atmospheric parameters from data collected by serial ascents from a line of rawinsonde stations normal to the general flow. They used a time-to-space conversion in order to be able to infer horizontal gradients. Three separate scales of motion were found besides the basic large-scale motion. The three scales reported were convective cells, convective bands, and large mesoscale motions of wavelength 200 to 300 km. It is the spatial and temporal changes of the motions of the third type that are emphasized in the present research.

By using data collected at 90-min intervals in a mesoscale network of special rawinsonde stations, Kreitzberg and Brown (1970) studied mesoscale circulations in a continental occulsion. They observed mesoscale features with space and time continuity on the order of a few hours and a few hundred miles as contrasted to synoptic features of which the continuity is on the order of days and many hundreds of miles. They showed that the variability of weather is related closely to mesoscale features within the cyclone-scale system.

Scoggins et al. (1972) examined the relationship of mesoscale systems to the synoptic features normally analyzed on weather maps. Both statistical and analytical approaches were used. The statistical approach did not isolate parameters that were statistically significant as indicators of the presence or absence of mesoscale systems for all seasons. However, some parameters indicated the presence of mesoscale systems during certain seasons. The analytical approach produced more conclusive results. From this approach they concluded that the relationships between meso- and synoptic-scale systems are defined best during seasons when the synoptic systems are defined well. They showed that it is possible to delineate areas but not specific locations where mesoscale systems should be present.

During February 1964, NASA conducted the first Atmospheric Variability Experiment (AVE I). Three-hour rawinsonde measurements were taken at the 30 regular rawinsonde stations in the southeastern United States during a 4-d period. Scoggins et al. (1973) used these unique data to study precipitation, wind variability, and internal zones of discontinuity. They showed that 80.8% of the stations where steady precipitation occurred during the AVE I experiment were in areas where the large-scale vertical motion was upward. Five methods of calculating vertical motion were used. The kinematic method applied at low altitudes in the atmosphere best delineated the rain and no-rain areas while the adiabatic

method applied at high altitudes provided the second best results. When compared to all methods applied at upper levels only, the adiabatic method was best.

In their study of zones of discontinuity, Scoggins et al. (1973) found that the intensity and slope of the zones varied greatly in 3 h. Internal zones of discontinuity were identified by using cross-section analysis of equivalent potential temperature. A frontogenetic function was used to study the variations and to identify those processes which caused the variations in the intensity of the zones of discontinuity. They showed that changes in the intensity of precipitation were correlated with the changes in slope and intensity of zones of discontinuity that they could observe by using 3-h data. Most of the zones studied changed so rapidly that they could not be followed with data taken at 12-h intervals. The conclusions that they reached using the AVE I data show that the variation of surface weather is related to atmospheric variability on a time scale less than 12 h.

Bosart (1973) used hourly precipitation reports to study the effect of mesoscale systems on the distribution of precipitation from winter storms moving along the east coast of the United States. He demonstrated that mesoscale phenomena influenced precipitation rates in the two cases studied. It can be seen in light of his work that mesoscale systems must be understood better in order to improve precipitation and flood forecasting.

c. Objectives

The main objective of this research is to use the unique AVE IIP data to study systems that cannot be analyzed adequately from routine data.

The specific objectives are to:

(1) Identify and follow mesoscale systems by using rawinsonde data taken at 3-h intervals;

(2) Examine changes in vertical motion at intervals of 3 h from the AVE IIP data, and relate the vertical motion fields to convective systems observed by radar;

(3) Determine the contribution of mesoscale systems to vertical motion; and

(4) Relate changes in the magnitude of vertical motion over 3-h intervals and compare with those over 12-h intervals to determine to what extent the more frequent soundings indicate significate features in the vertical motion field.

3. DATA AND SYNOPTIC CONDITIONS

a. AVE II Pilot Experiment

The data used in this study were obtained for NASA during their second Atmospheric Variability (Pilot) Experiment (AVE IIP). The experiment was conducted during the period of 1200 GMT 11 May 1974 to 1200 GMT 12 May 1974. Soundings were taken at 54 rawinsonde stations at 3-h intervals during the experiment. Figure 1 shows the locations and station identifiers* of the participating stations.

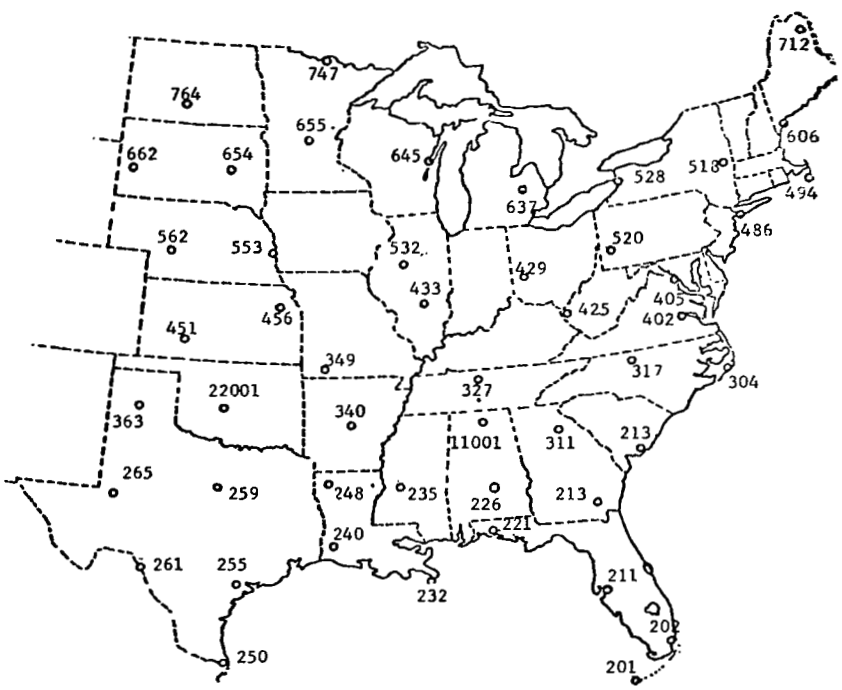

Fig. 1. Location of rawinsonde stations for AVE IIP.

*Station names are given in Appendix I.

Personnel from each station forwarded the original records of each rawinsonde flight to the Marshall Space Flight Center. Personnel from Texas A&M University, under the supervision of NASA personnel, extracted the data from the original records and punched them into cards. First differences of the data were calculated and errors corrected. The cards were sent to Texas A&M University where the data reduction was completed.

A master reduction program designed to provide the most accurate meteorological, vertical soundings possible was developed at Texas A&M. The program differs from the standard reduction procedures in several ways. The vertical profiles calculated have thermodynamic information for every pressure contact or approximately 10-mb intervals. The winds were calculated at 30-s intervals rather than the usual 2- to 4-min intervals. The winds at 30-s intervals were smoothed and then interpolated for each pressure contact. The above procedure not only produces winds that are representative for thinner layers in the atmosphere, but also insures that the wind is matched with thermodynamic quantites for the same level. Details of the data reduction procedure are given by Fuelberg (1974).

In order to eliminate as many errors as possible, first differences also were calculated for the sounding data for each pressure contact. Extensive and careful manual checking of the soundings and first differences was carried out and all detectable errors corrected. The corrected soundings were stored on magnetic tape.

The stated approximate accuracy of the data in RMS values (Fuelberg, 1974) is as follows:

(1) Temperature: 1°C.

(2) Pressure: 1.4 mb from the surface to 400 mb, 1.1 mb from 400 to 100 mb, and 0.7 mb above 100 mb.

(3) Humidity: 10%.

(4) Pressure altitude: 10 gpm at 500 mb, 20 gpm at 300 mb, and 50 gpm at 50 mb.

(5) Winds: 1.5 m s^{-1} and 5° at 700 mb, 2.5 m s^{-1} and 8° at 500 mb, and 4.5 m s^{-1} and 10° at 300 mb.

The reduction scheme used to obtain the AVE IIP soundings has produced data that are more accurate and have a much greater information content than operational soundings routinely available. Every effort was made during AVE IIP to retain as much resolution as possible in the vertical soundings.

b. Synoptic conditions

The synoptic pattern at 1200 GMT 11 May 1974 was made up of a retreating cold air mass over the northeast United States , fresh polar air penetrating the Northern Plains States, and moist air moving up the Mississippi Valley. The two major weather-producing features were a polar cyclone in central Minnesota and a warm-sector cyclone centered just off the Texas Gulf Coast. Surface, 850-, 500-, and 300-mb charts are shown in Figs. 2, 3, and 4 for 1200 GMT 11 May 1974 and 0000 and 1200 GMT 12 May 1974.

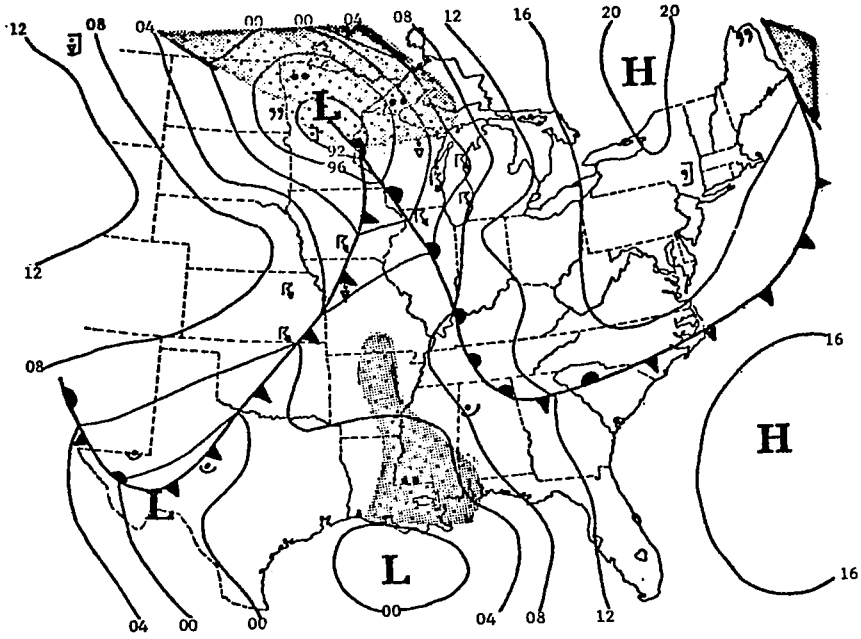

(a) Surface

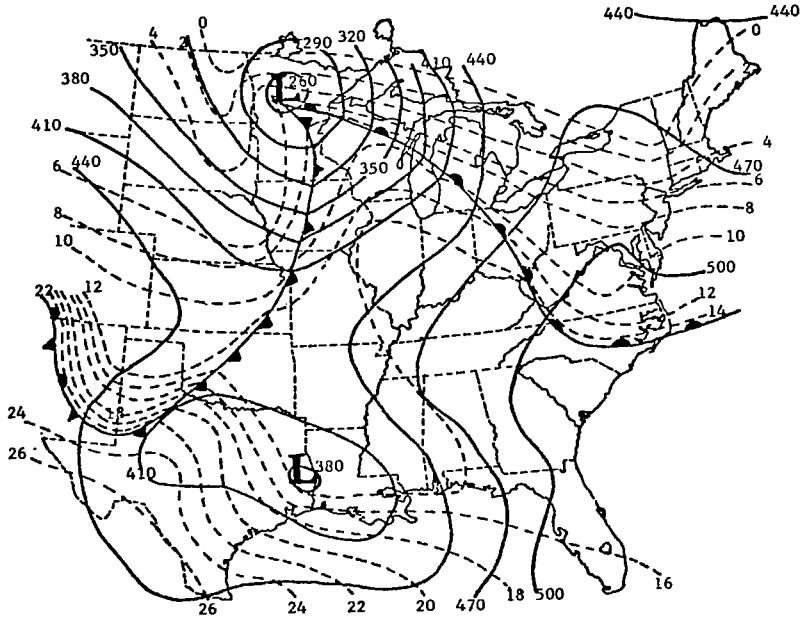

(b) 850 mb

Fig. 2 Synoptic charts for 1200 GMT 11 May 1974.

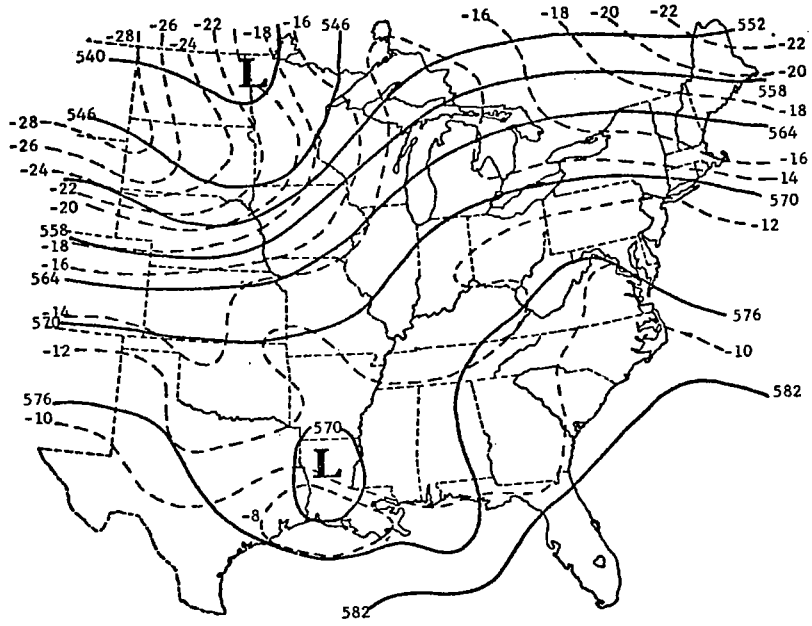

(c) 500 mb

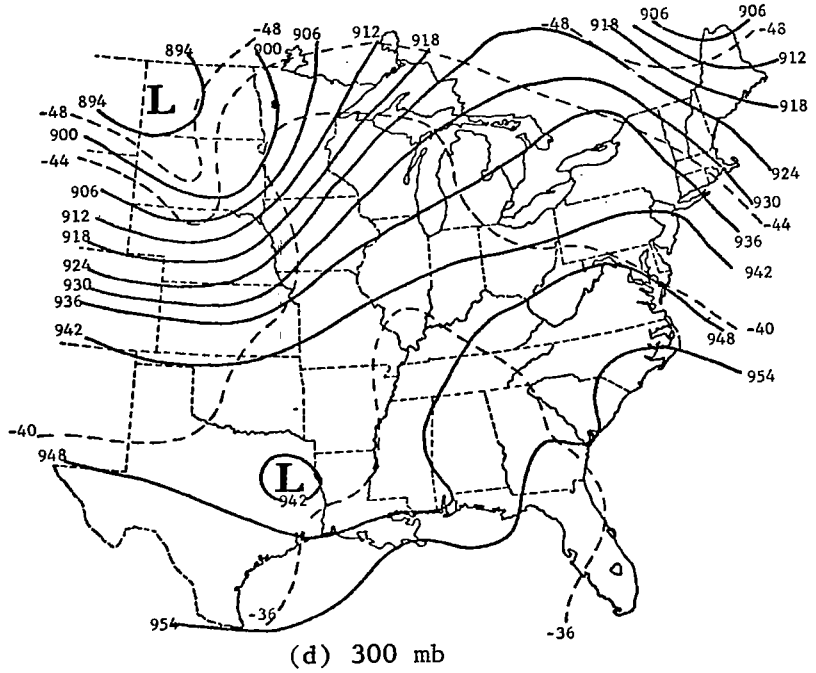

(d) 300 mb

Fig. 2. Continued.

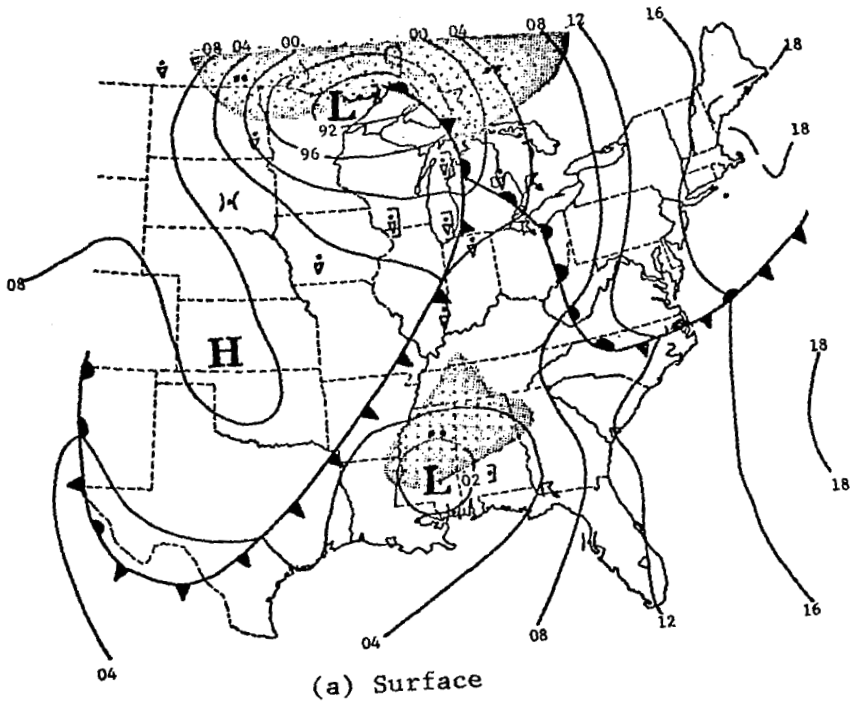

(a) Surface

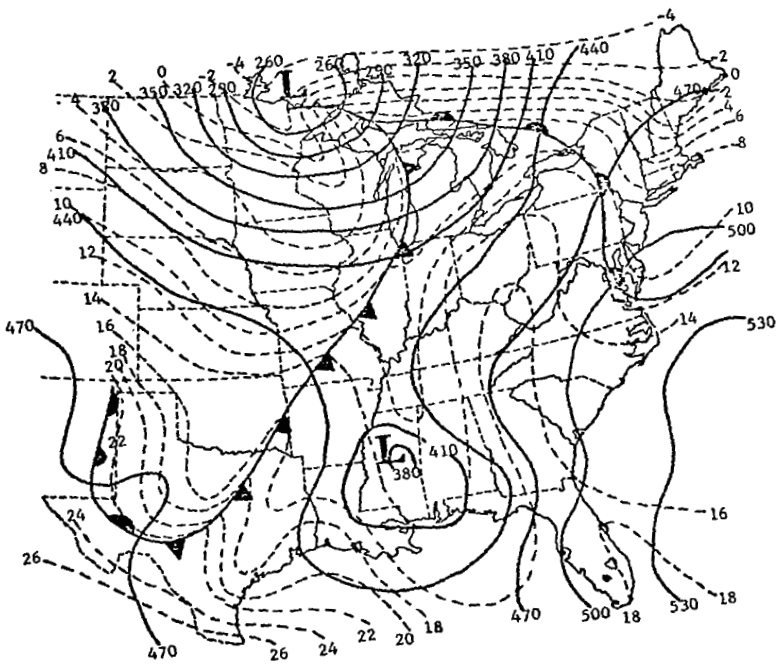

(b) 850 mb

Fig. 3. Synoptic charts for 0000 GMT 12 May 1974.

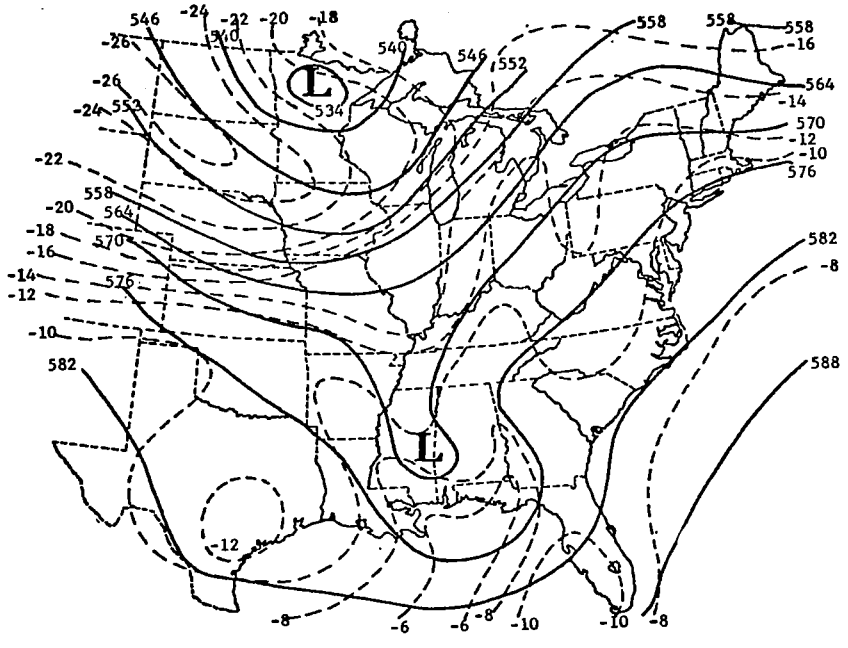

(c) 500 mb

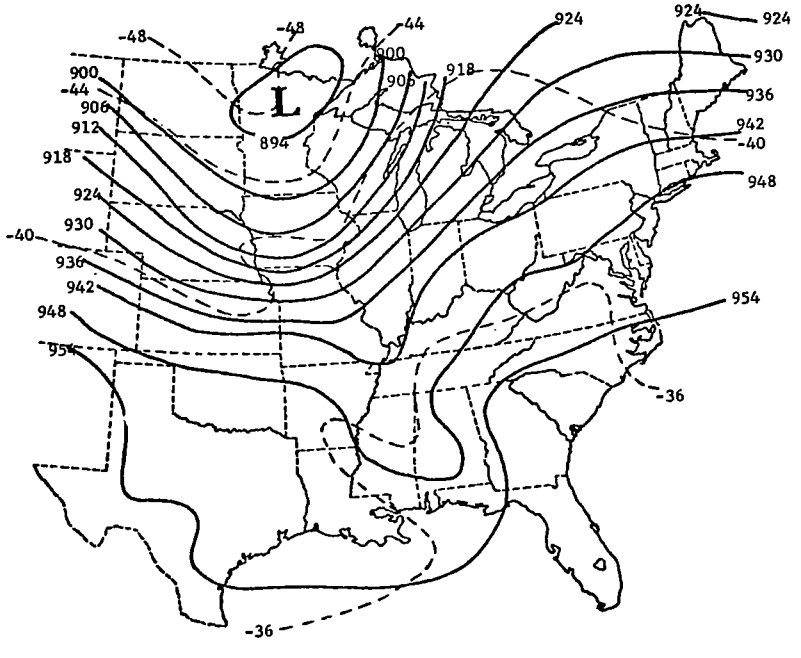

(d) 300 mb

Fig. 3. Continued.

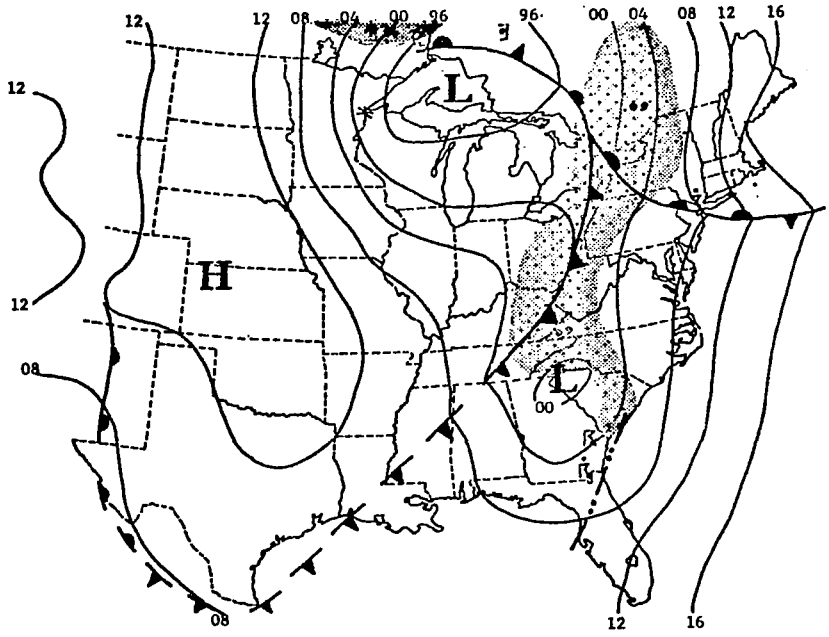

(a) Surface

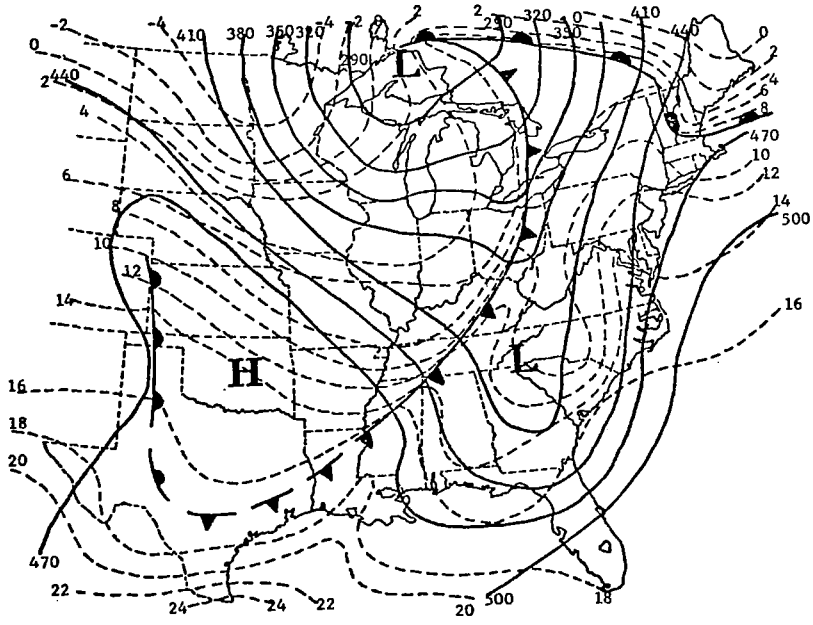

(b) 850 mb

Fig. 4, Synoptic charts for 1200 GMT 12 May 1974.

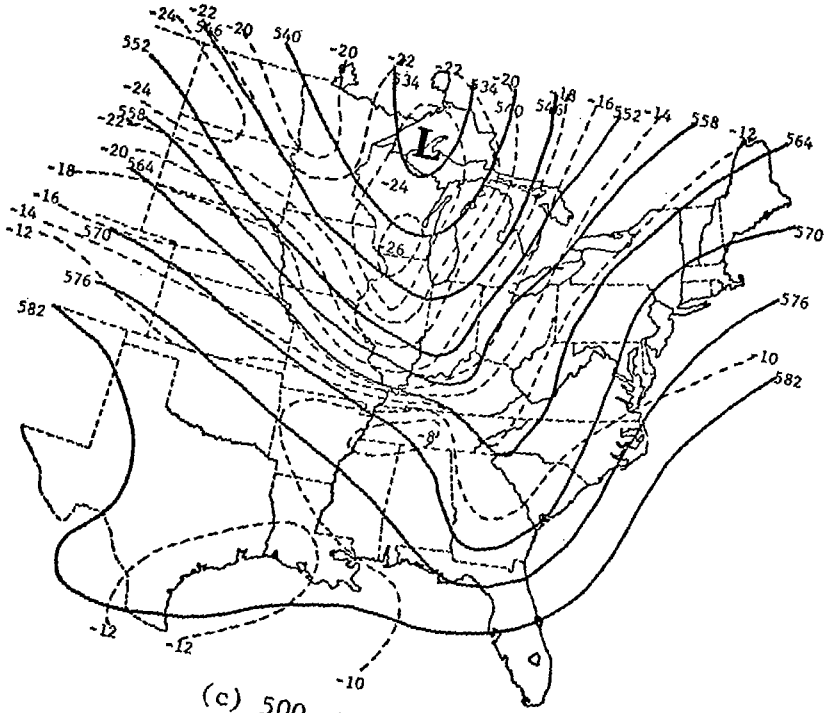

(c) 500 mb

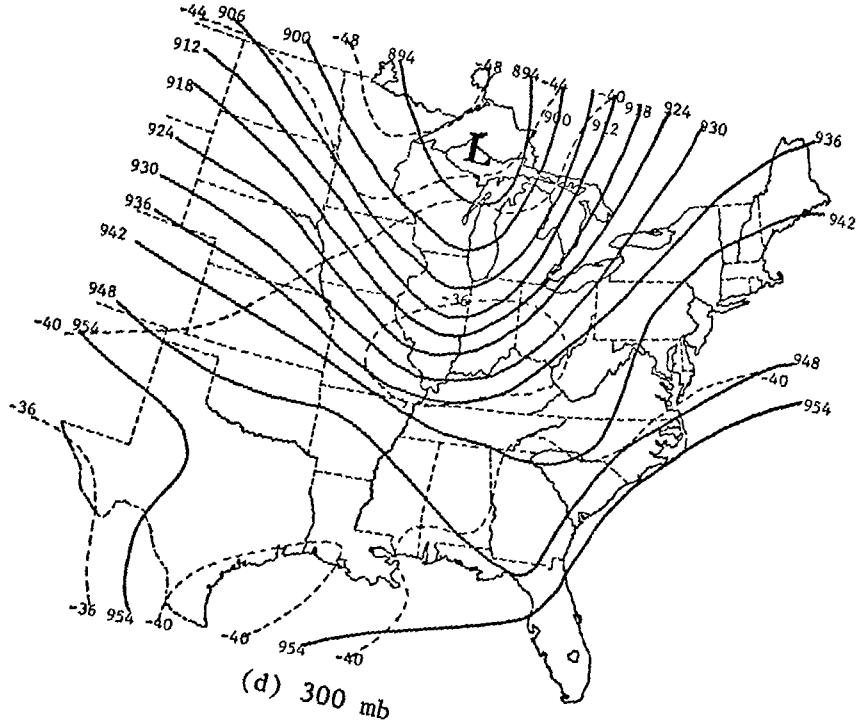

(d) 300 mb

Fig. 4. Continued.

During the 24-h period of the experiment, the northern cyclone moved to the eastern end of Lake Superior and the southern low-pressure area moved to western North Carolina. By 1200 GMT 12 May 1974, the polar outbreak covered most of the eastern United States. Radar echoes were restricted mainly to the warm sector during the period except for an area of showers that developed in the cold air and moved across the North Central States.

The circulation of the two cyclones was well defined on the standard isobaric charts. The polar cyclone had a closed circulation through the 500-mb level. A 500-mb trough that extended southward from the polar cyclone moved east at about 6 m s^{-1} and deepened slightly during the period of the experiment. The AVE IIP data also showed several disturbances of shorter wavelength than the polar cyclone moving across the area of interest.

The warm segment of the polar front is fairly well-defined during the entire experiment; however, due to frontolysis, the cold segment south of the middle Mississippi Valley was difficult to locate during the second half of the period.

4. ANALYTIC APPROACH

a. Isentropic charts

Potential temperature, θ, was chosen as the vertical coordinate for this study since isentropic charts present a more coherent pattern of flow and moisture than height or pressure charts (Rossby et al., 1937). The time coherence of systems on isentropic charts greatly simplifies the task of evaluating changes in atmospheric properties.

During adiabatic processes the potential temperature of a parcel of air is conserved. Diabatic effects such as condenstaion and radiation may cause the potential temperature of a parcel to change. Rossby et al. (1937), Namias (1940), and others have pointed out that the potential temperature is conservative, except in large precipitation areas, for at least a few days.

In order to produce isentropic charts, a computer program was developed to convert from pressure to potential temperature coordinates. The data were converted to potential temperatures at 8 K intervals beginning at 300 K. The rawinsonde data for each pressure contact were scanned and when a selected potential temperature fell between two pressure contacts, the measured parameters were interpolated linearly to the proper potential temperature. The pressure difference between contacts was about 10 mb; therefore, linear interpolation was sufficiently accurate. When adiabatic or superadiabatic lapse rates were encountered, the highest level where the

potential temperature occurred was chosen. This seems reasonable since absolutely unstable regions should not exist over a long period of time. After the interpolation was complete all parameters for the isentropic levels were stored on magnetic tape.

Isentropic charts were constructed at 8 K intervals beginning at 300 K and ending at 340 K. The objective analysis scheme developed by Barnes (1964) was used to interpolate the rawinsonde data (now in potential temperature coordinates) to a grid (Fig. 5) with approximately 158-km spacing between grid points. This interval

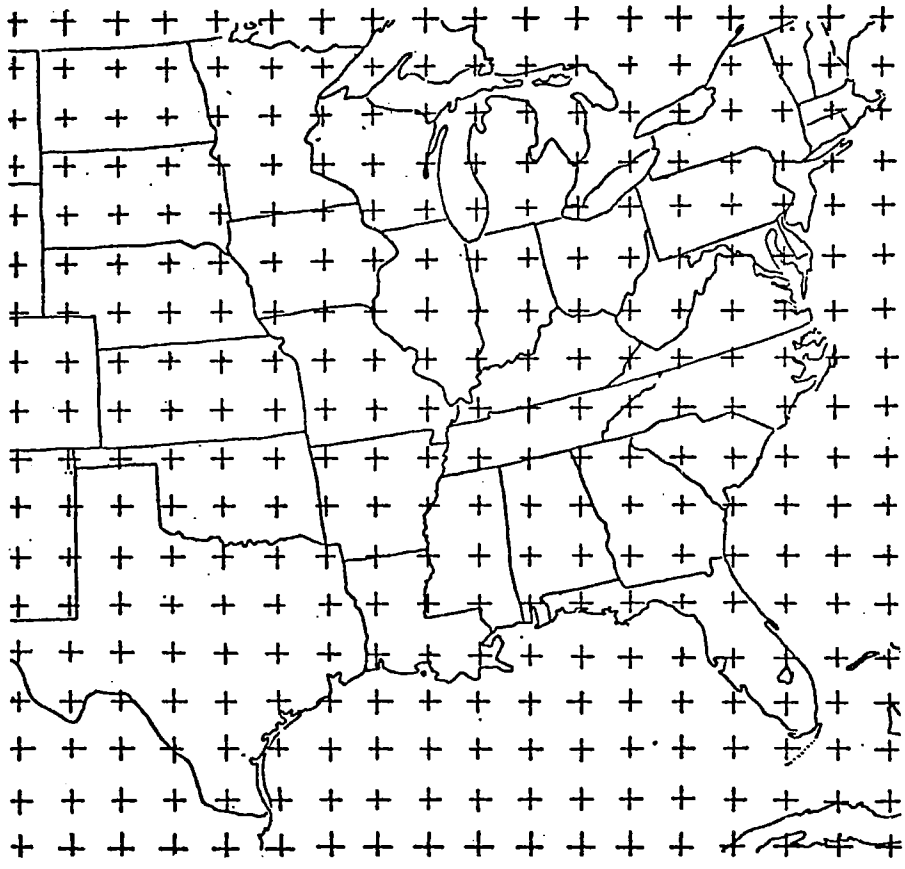

Fig. 5. Grid used for numerical computations.

is small enough to represent the horizontal detail that can be measured by the randomly spaced rawinsonde stations (Barr et al., 1971). Barnes' method makes successive corrections to a first-guess field. The first guess for this study was taken to be zero and four iterations were allowed. The data from each rawinsonde station were allowed to influence grid-points within a radius of four grid distances.

Fields of pressure, height, and wind were analyzed. Then, by use of the expression

$$Q = \left(\frac{\Delta v}{\Delta x} - \frac{\Delta u}{\Delta y} \right) + f$$

absolute vorticity was calculated. Q represents absolute voritcity, u and v the horizontal wind components, and f the coriolis parameter. The absolute vorticity was multiplied by $\Delta\theta/\Delta p$ to obtain the potential vorticity. Backward differences were used in the calculation of $\Delta\theta/\Delta p$.

After all parameters had been calculated, the pressure field was contoured by use of a computer scheme from the National Center for Atmospheric Research. The other charts were printed on the grid with values to the left of each grid point.

b. Vertical motion

Saucier (1955) states that the calculation of vertical motion is one of the most practical uses of isentropic charts. To arrive at an expression for vertical motion in isentropic coordinates, the

total derivative may be written as

$$\left(\frac{dz}{dt}\right)_\theta = \left(\frac{\partial z}{\partial t}\right)_\theta + \left(\frac{dx}{dt}\right)_\theta \left(\frac{\partial z}{\partial x}\right)_\theta + \left(\frac{dy}{dt}\right)_\theta \left(\frac{\partial z}{\partial y}\right)_\theta \quad (1)$$

where the subscript θ refers to constant potential temperature. Let the wind components of the θ-surface be represented by u_θ and v_θ, where $u_\theta = (dx/dt)_\theta$ and $v_\theta = (dy/dt)_\theta$. With this notation (1) becomes

$$\left(\frac{dz}{dt}\right)_\theta = \left(\frac{\partial z}{\partial t}\right)_\theta + u_\theta\left(\frac{\partial z}{\partial x}\right)_\theta + v_\theta\left(\frac{\partial z}{\partial y}\right)_\theta \quad (2)$$

where $(\partial z/\partial x)_\theta$ and $(\partial z/\partial y)_\theta$ represent the slopes of the isentropic surface in the x- and y-directions, respectively. The first term on the right-hand side of (1) represents the local time rate-of-change of the height of the isentropic surface, and $(dz/dt)_\theta$ is the vertical motion of a parcel on the θ-surface.

It is easy to evaluate (2) from objectively analyzed height and wind data. Backward differences were used to obtain $(\partial z/\partial t)_\theta$ and, therefore, this quantity represents an average rate of change for the past 3 h. This rate was used as if it were instantaneous. All other terms were evaluated by using their instantaneous values at the time the measurements were taken.

In order to interpret (2) more easily notice that

$$u_\theta \left(\frac{\partial z}{\partial x}\right)_\theta + v_\theta \left(\frac{\partial z}{\partial y}\right)_\theta = V_\theta \left(\frac{\partial z}{\partial s}\right)_\theta$$

where V_θ is the wind speed and s is the direction downwind along the streamlines. Also, $(\partial z/\partial t)_\theta$ may be written as $-V_I(\partial z/\partial s)_\theta$,

where V_I represents the speed of movement of the isentropic surface in the s-direction. This, of course, assumes that the surface moves without change of shape. With these substitutions (2) becomes

$$\left(\frac{dz}{dt}\right)_\theta = \left(V_\theta - V_I\right)\left(\frac{\partial z}{\partial s}\right)_\theta .$$

This is the form given by Saucier (1955). Now it can be seen that the vertical motion calculated from (2) takes into account parcels of air moving on a sloping surface as well as the movement of the surface.

One difficulty encountered when calculation began was large apparent movements of the isentropic surfaces below 1500 m due to diurnal radiational effects. The 300 K and 308 K surfaces were the only ones that were within 1500 m of Earth's surface, and only a small percentage of the area on these two charts was affected. System movement, $(\partial z/\partial t)_\theta$, was assumed zero if the surface was within 1500 m of Earth's surface. This procedure did not affect calculations of motion at the higher levels since the diabatic effects were confined to the lower levels.

The isentropic method used to calulate vertical motions in this study is superior to other methods in several ways. Since each level is calculated independently, this method does not require a lower boundary vertical motion or the evaluation of divergence of the wind field as in the kinemetic method. Unlike the standard

adiabatic method, the isentropic method does not require specification of the temperature lapse rate through the level where vertical motion is calculated. One of the greatest advantages of the isentropic method is the great simplicity of evaluation of vertical motion.

5. RESULTS

a. Temporal and spatial changes in vertical motion

Vertical motion was calculated for six levels, but only one level will be shown. Selected vertical cross sections will be shown in order to present the vertical consistency of the patterns of vertical motion.

The vertical motion fields on the 308 K surface will be shown because that level best depicts the mid-tropospheric vertical motions for this synoptic situation. One problem with presenting vertical motions on isentropic surfaces is the variation in altitude of the surfaces. Contours of pressure are shown on the isentropic charts so the reader can infer slope and a relative vertical position of the surfaces.*

Vertical motions computed from (2) and radar echoes are shown in Figs. 6 through 13. Areas of radar echoes were obtained from the National Weather Service's radar summary chart and supplemented by photographic and written logs from radar stations. The largest vertical motion calculated on the 308 K surface was 18 cm s^{-1}, while 22 cm s^{-1} was the largest magnitude calculated in the entire study. These magnitudes appear reasonable when compared to previous studies but are larger than those generally associated with synoptic systems. Kreitzberg and Brown (1970) showed vertical motions of 20 cm s^{-1} calculated by use of the kinematic method. They also state

*Relationships between pressure and height are shown in Appendix II.

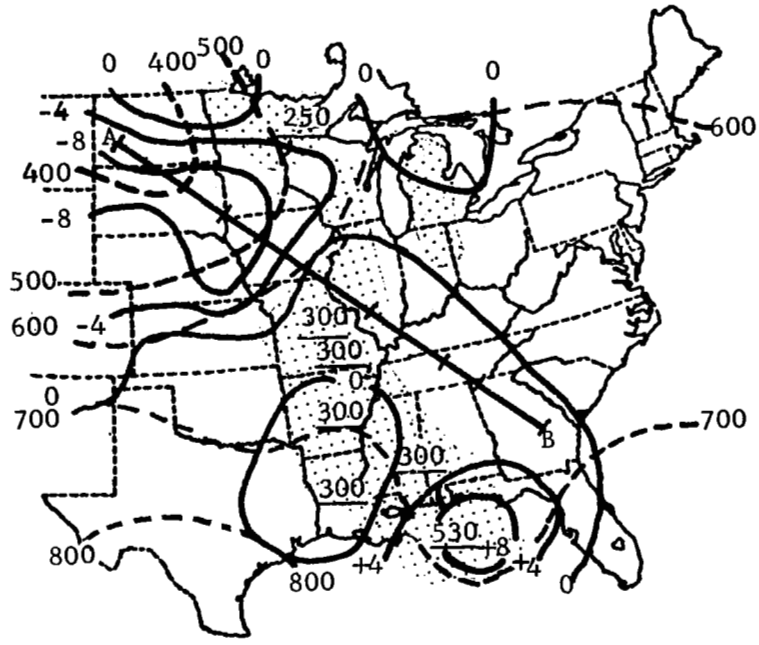

Fig. 6. Vertical motion (cm s^{-1}) on the 308 K potential-temperature surface for 1500 GMT 11 May 1974. Areas of radar echoes are stippled with echo tops indicated in hundreds of feet by underlined numbers, and pressure contours (mb) are represented by dashed lines.

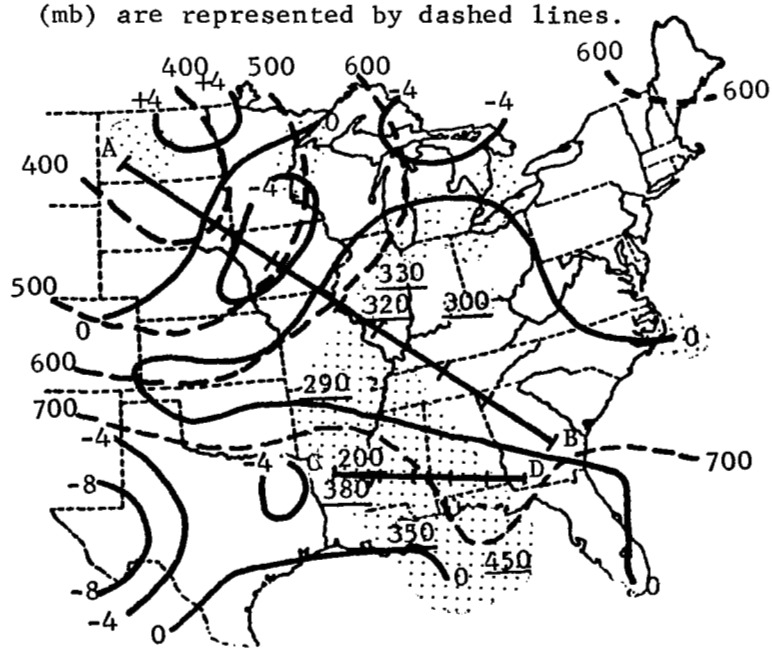

Fig. 7. Same as Fig. 6 except for 1800 GMT 11 May 1974.

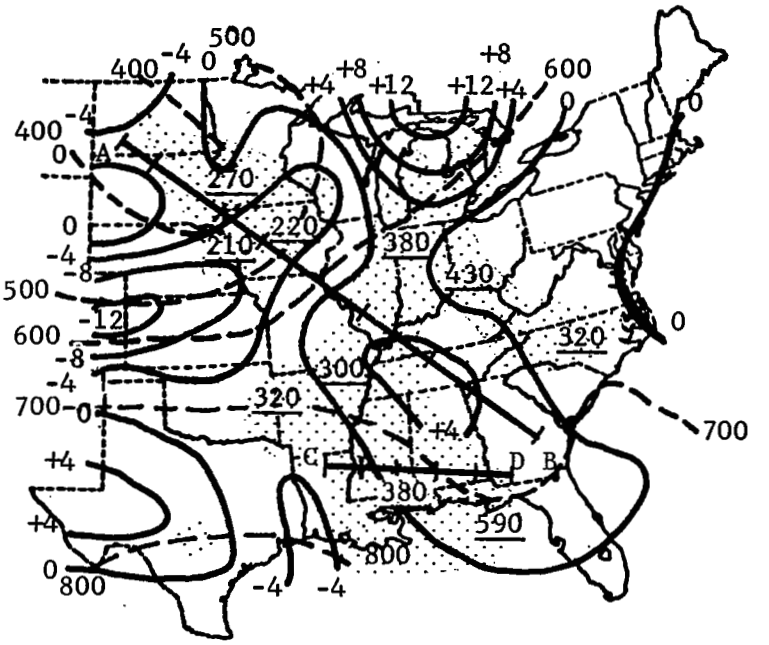

Fig. 8. Same as Fig. 6 except for 2100 GMT 11 May 1974.

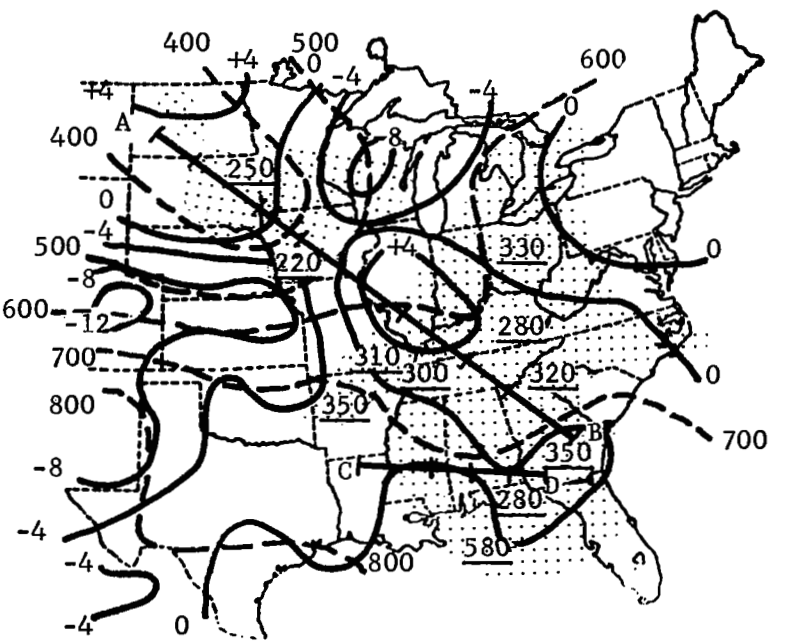

Fig. 9. Same as Fig. 6 except for 0000 GMT 12 May 1974.

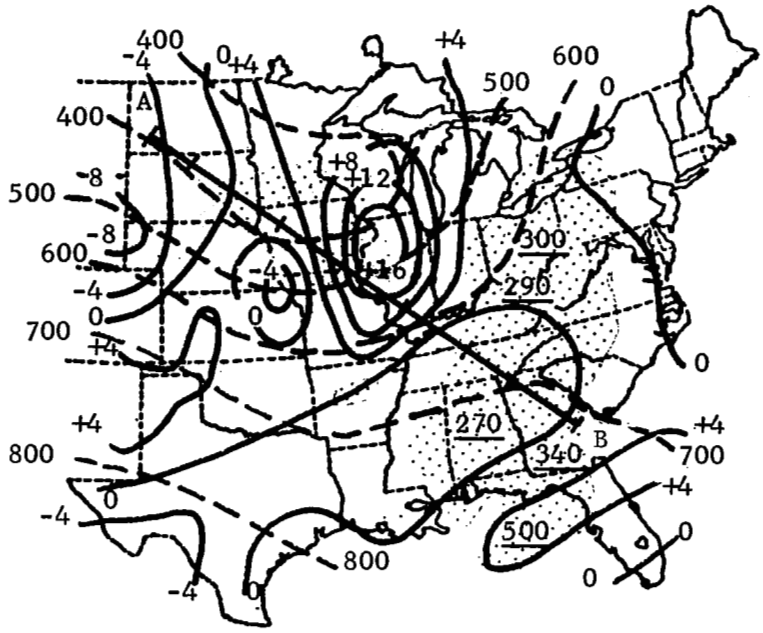

Fig. 10. Same as Fig. 6 except for 0300 GMT 12 May 1974.

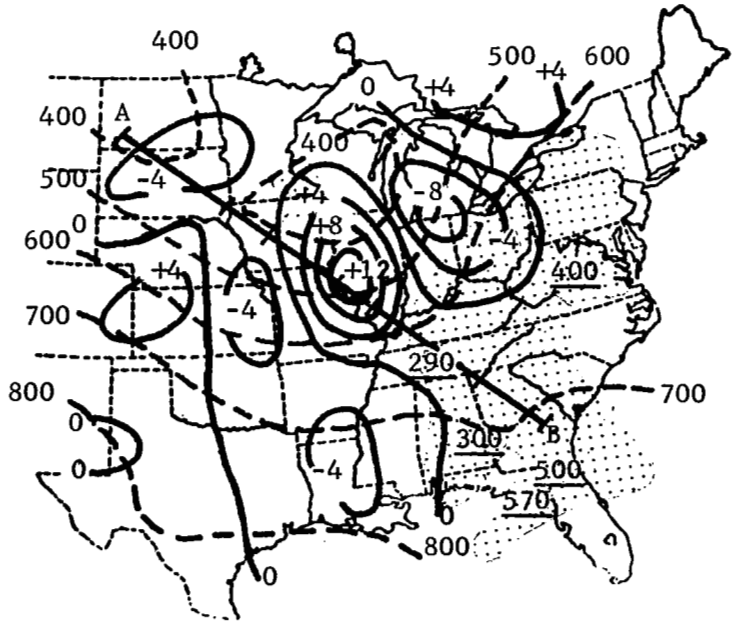

Fig. 11. Same as Fig. 6 except for 0600 GMT 12 May 1974.

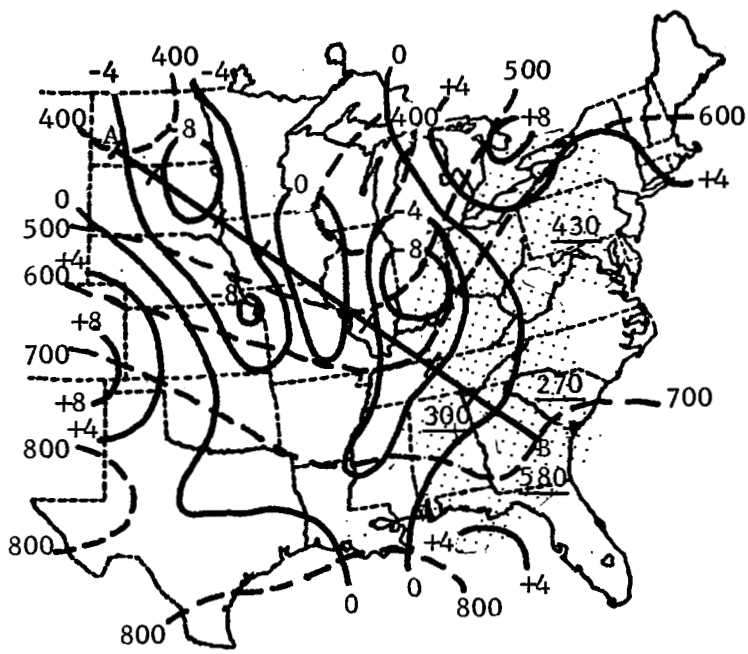

Fig. 12. Same as Fig. 6 except for 0900 GMT 12 May 1974.

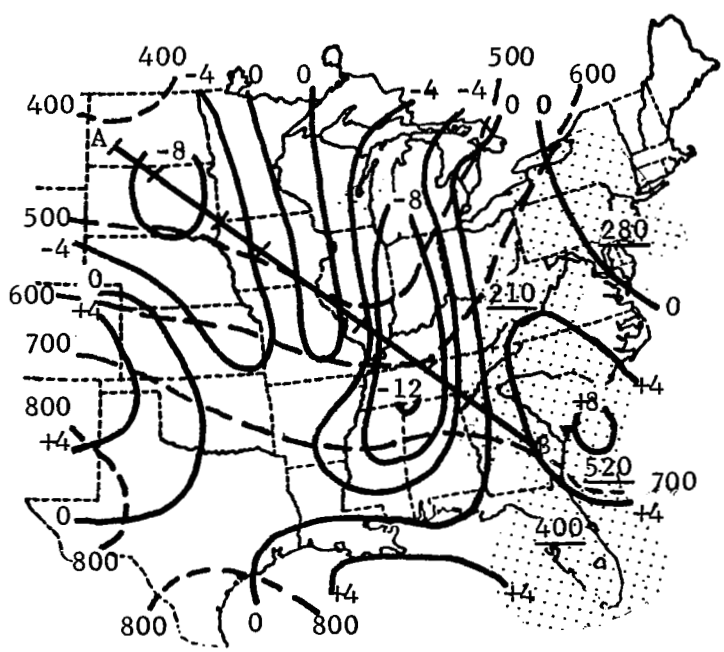

Fig. 13. Same as Fig. 6 except for 1200 GMT 12 May 1974.

that the motions they showed had been reduced by a certain percentage of the 200-mb vertical motion. Petterssen (1956) shows vertical motions in the mid-troposphere as strong as 18 cm s^{-1}.

1. Radar echoes versus vertical motion

When comparing the radar echoes to the fields of vertical motion, it should be remembered that the areas delineated on the radar summary charts are not completely covered by convective cells, and the vertical motion is for one level in the middle troposphere.

Figures 6 through 13 show that areas of convection generally were associated with positive vertical motion in the mid-troposphere. However, upward motion alone does not necessarily imply convection because of moisture and other considerations.

In areas where the vertical motion was downward in excess of 4 cm s^{-1} on the 308 K surface, convective cells did not penetrate this surface. The only apparent exception to this occurred in the eastern part of the shower area in Nebraska, Iowa, and Wisconsin at 2100 GMT 11 May and 0000 GMT 12 May. The maximum tops of showers in these areas penetrated the 308 K level by as much as about 2 km. However, only isolated cells appear to have extended upward through the 4 cm s^{-1} downward motion and, in general, the strong down motions appeared to halt the vertical growth of the convection.

Figure 11 shows that along the frontal zone at 0600 GMT on 12 May, the area of Indiana and Ohio covered by the downward motion had light rainshowers while heavy rainshowers and thundershowers were present over western Kentucky where the vertical motion was

upward. Cincinnati reported no change in intensity of the light showers below the downward area, but increasing intensity for the convection under the area of upward motion was reported at Evansville. By 0900 GMT the short-wave cell of downward motion had moved southward and was over the Evansville area where the intensity of the convection was decreasing.

Again at 0900 GMT the most intense convection was observed in areas where the vertical motion was upward in the mid-troposphere. It appears that convection at 0600 GMT and 0900 GMT below the downward-motion area in Indiana, Ohio, and Kentucky may have penetrated the 308 K level where the downward vertical motion reached 4 cm s^{-1}. Inspection of the radar observations at Evansville and Cincinnati shows that cells with maximum height were near the 4 cm s^{-1} isoline. Radar information was not available to show the exact tops of cells inside this area, but it appears that the convection did not penetrate the 308 K level.

Figure 14 shows a cross section along line AB in Fig. 8. For this and following cross sections, see Appendix II for relationships between pressure and height. The radar summary shows that the area of convection ended within a short distance of the point where the downward motion exceeded 4 cm s^{-1} over a deep layer. The bases of the convective clouds in the cold air were much lower than the 300 K surface, which is the lowest level where vertical motion was calculated. Extremely unstable air in the 2-km layer next to Earth's surface apparently provides an explanation of the

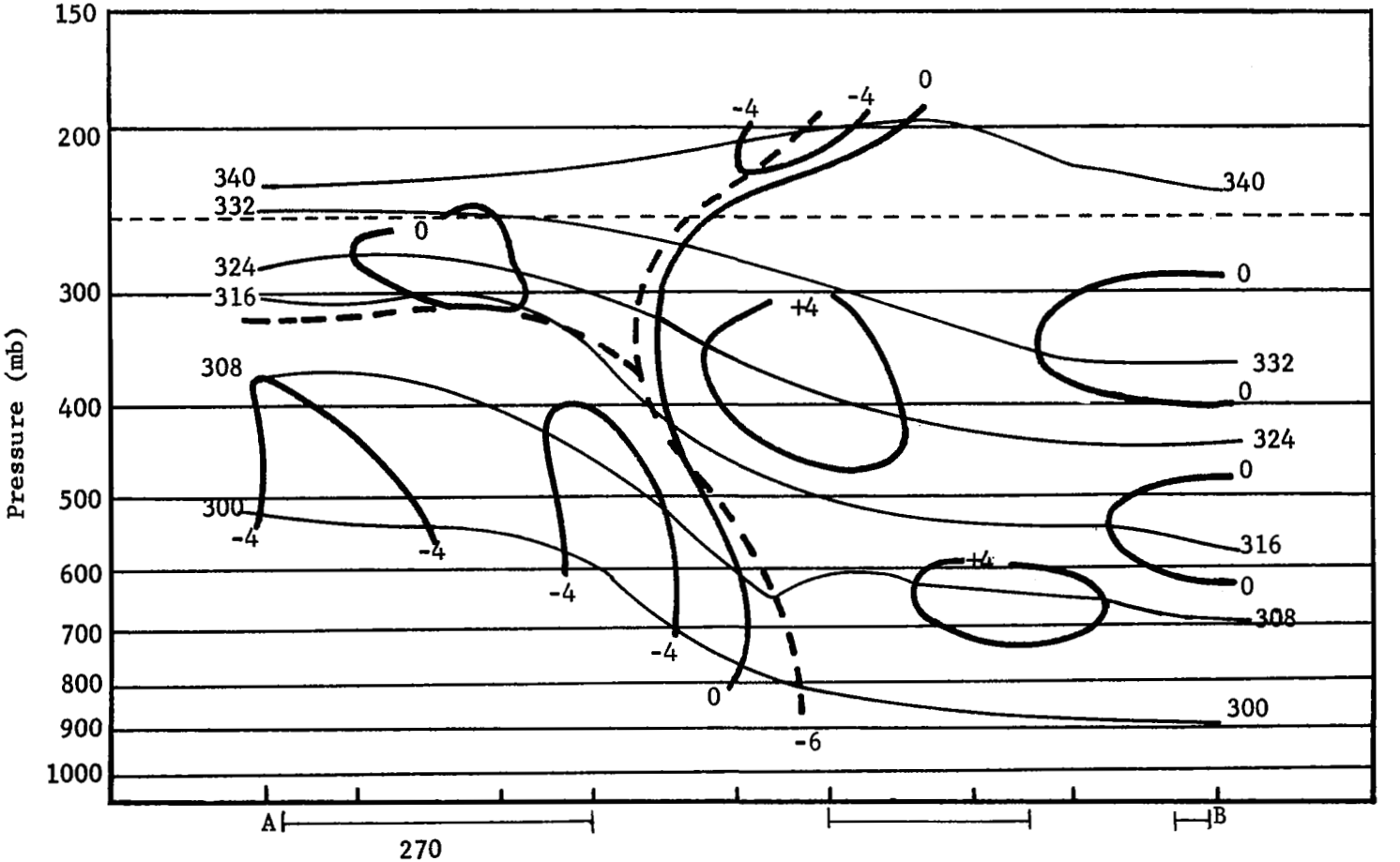

Fig. 14. Cross section along line AB in Fig. 8 (2100 GMT 11 May 1974.) Vertical motion (cm s^{-1}) is represented by heavy solid lines, potential temperature (K) by thin solid lines, and fronts and tropopauses by dashed lines. Bars under cross section indicate portions of the cross section in radar summary areas. Numbers under bar give reported cloud heights in hundreds of feet.

convection, but mid-tropospheric downward motion appears to explain why the convection ceased several miles behind the surface front. Also, the tallest cell along the cross section occurred in the area where the mid-tropospheric downward motion had a magnitude less than 4 cm s^{-1}.

A cross section along line AB in Fig. 9 is shown in Fig. 15. Again it can be seen that the height of the top of the cells was related to the intensity of the downward motion. The radar summary again showed that convection ended within a short distance of the grid point where the downward motion reached 4 cm s^{-1} over a deep layer in the mid-troposphere.

The magnitudes and gradients of the vertical motions diminished away from the cold front, but even in the warm sector the vertical motion patterns appear consistent with the observed convection. Cross sections along line CD of Figs. 7, 8, and 9 are shown in Fig. 16. In Fig. 16a, the convection near point C has a maximum height of 6.1 km, while near grid point 3, where the lower troposphere has upward motion, the convection extends to 11.6 km. The maximum echo tops shown in Fig. 16b are located just west of the area where the mid-tropospheric motion had the greatest upward magnitude. As the convective area moved ahead of the surface front, the convection ended near the place where the tropospheric vertical motion changed to downward.

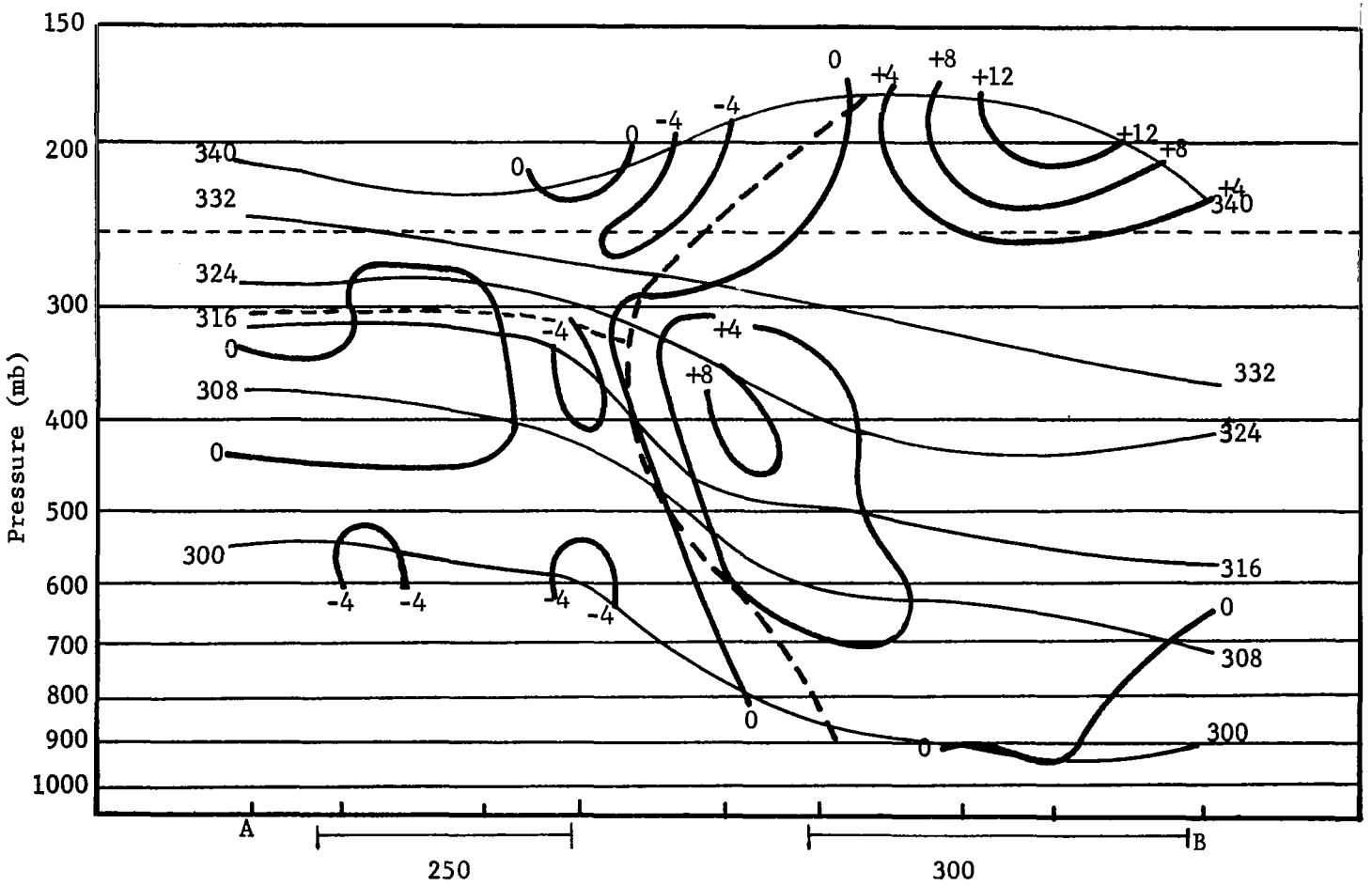

Fig. 15. Cross section along AB in Fig 9 (0000 GMT 12 May 1974). See Fig. 14 for explanation of legend.

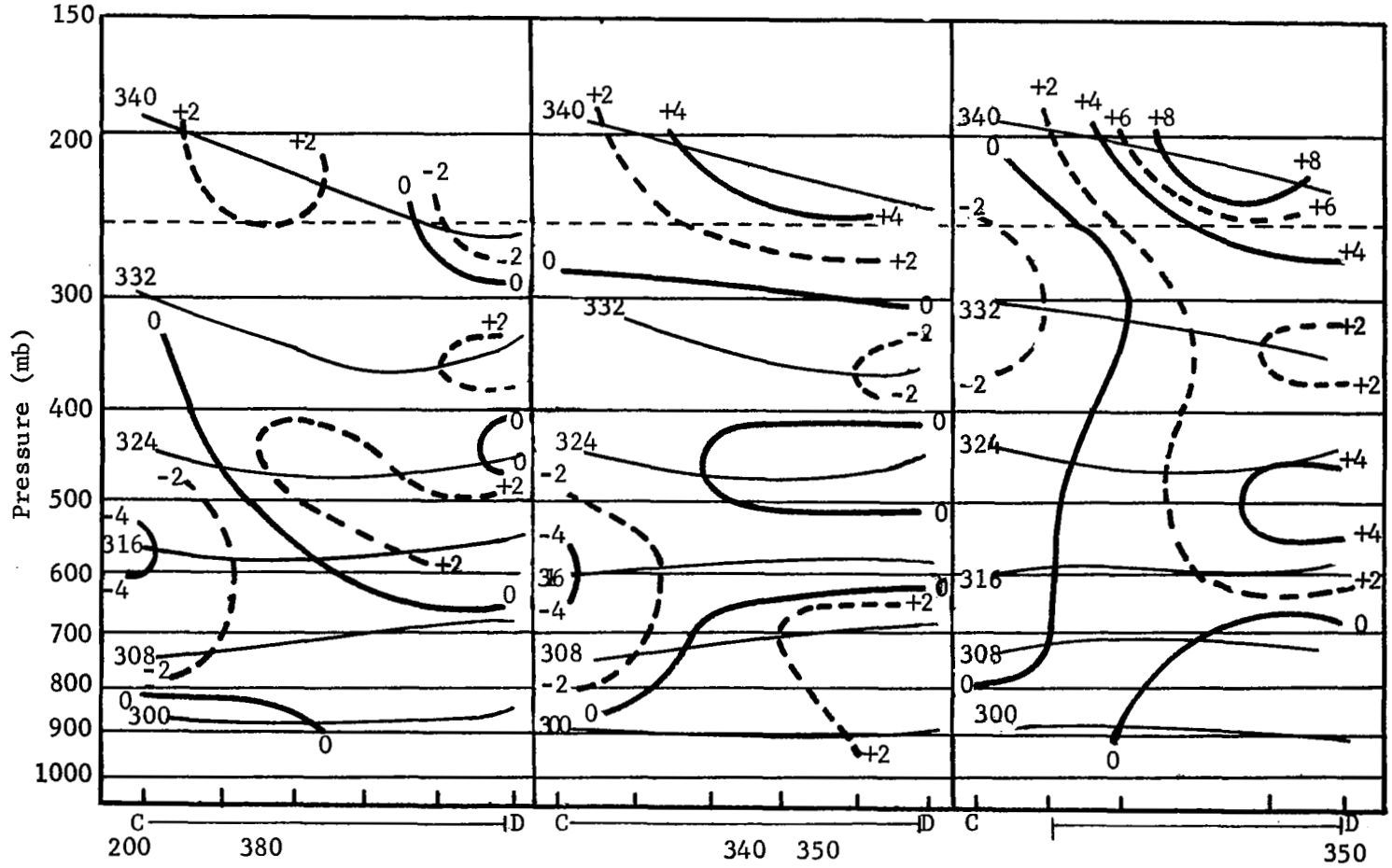

Fig. 16. Cross sections along line CD in Figs. 7, 8, and 9, respectively, 11 and 12 May 1974. Constructed similarly to Fig. 14 except fronts and tropopauses are not shown and dashed lines indicate intermediate values of vertical motion.

Figures 17 through 20 show cross sections along line AB of Figs. 10 through 13, respectively. As before, downward motion in excess of 4 cm s^{-1} apparently halted the growth of convective clouds in the vertical. Figures 19 and 20 show downward motion over great vertical depths; by referring to Figs. 12 and 13, one can see that no convective clouds were reported in these areas of negative vertical motion.

The above examples of the vertical motion fields, calculated by using the isentropic method, demonstrate that convective activity was associated with areas of large-scale vertical motion in this instance. An investigation of the relationship of the areas of vertical motion to other kinematic fields now will be presented.

2. Kinematic fields

The most obvious characteristic of the vertical motion fields below the tropopause level was the intense gradient of vertical motion in the frontal zone and the weak gradient away from frontal zones. One of the most interesting features of the vertical motion field during the experiment was the appearance of a short-wavelength pattern at 0600 GMT 12 May. This pattern, with a wavelength of approximately 600 km, persists to the end of the experiment although it had weakened by the last observation time. Short-wavelength troughs also are identifiable on constant-pressure charts during this time period. Figures 21 through 24 show observed wind fields and absolute vorticity for the 308 K surface that correspond to the vertical motion of Figs. 10 through 13

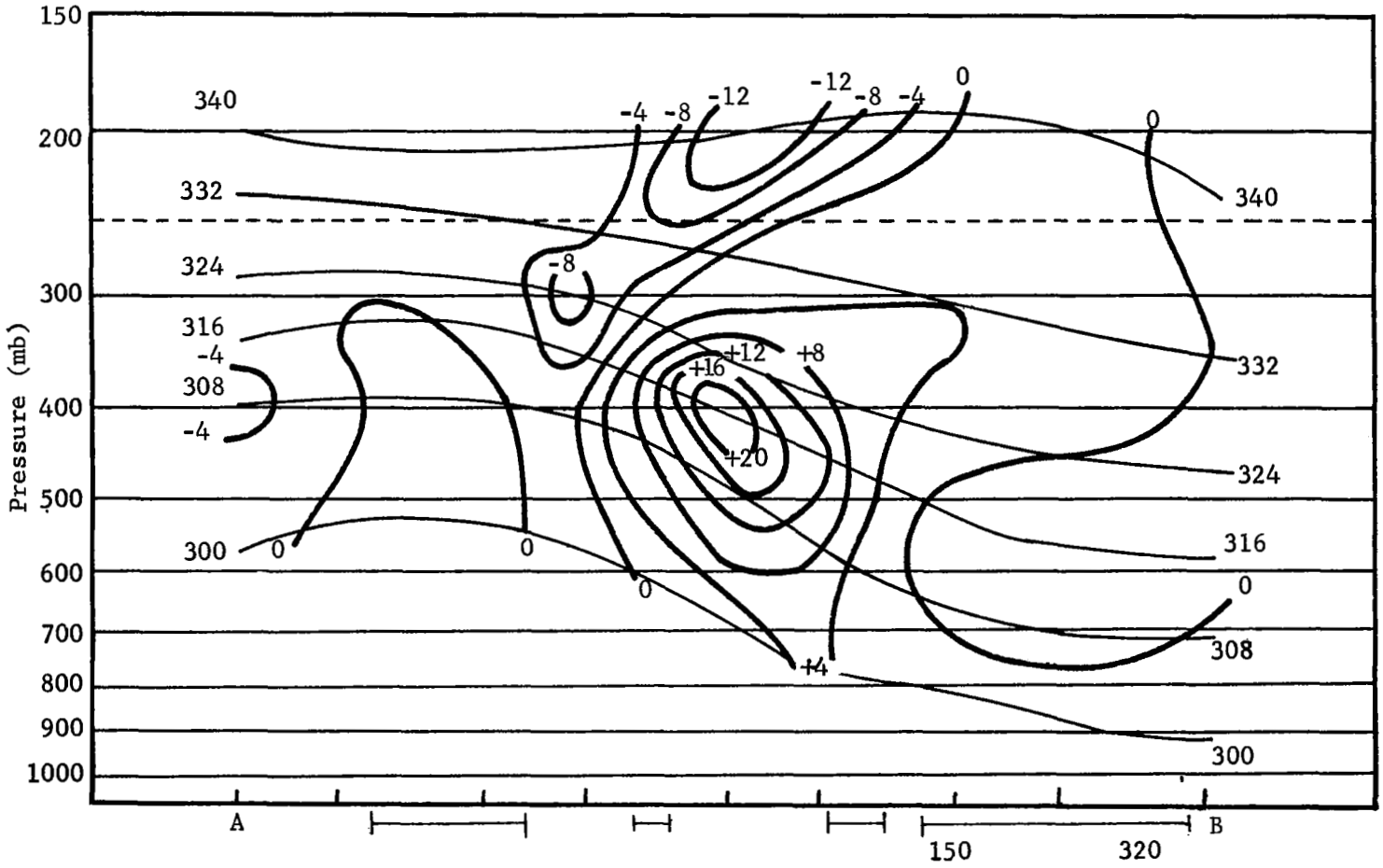

Fig. 17. Cross section along line AB in Fig. 10 (0300 GMT 12 May 1974). Constructed similarly to Fig. 14 except fronts and tropopauses are not shown.

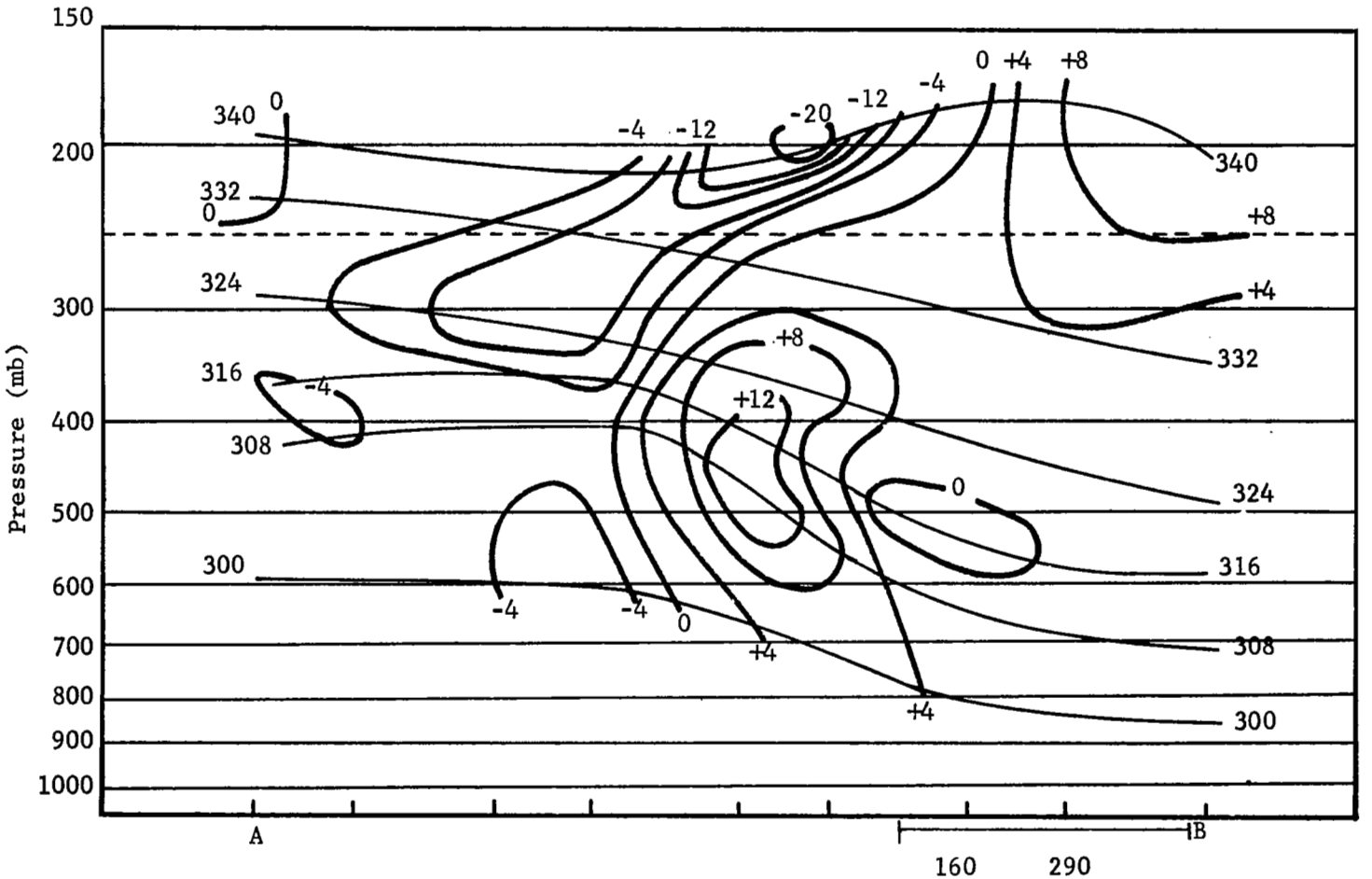

Fig. 18. Cross section along line AB in Fig. 11 (0600 GMT 12 May 1974). Constructed similarly to Fig. 14 except fronts and tropopauses are not shown.

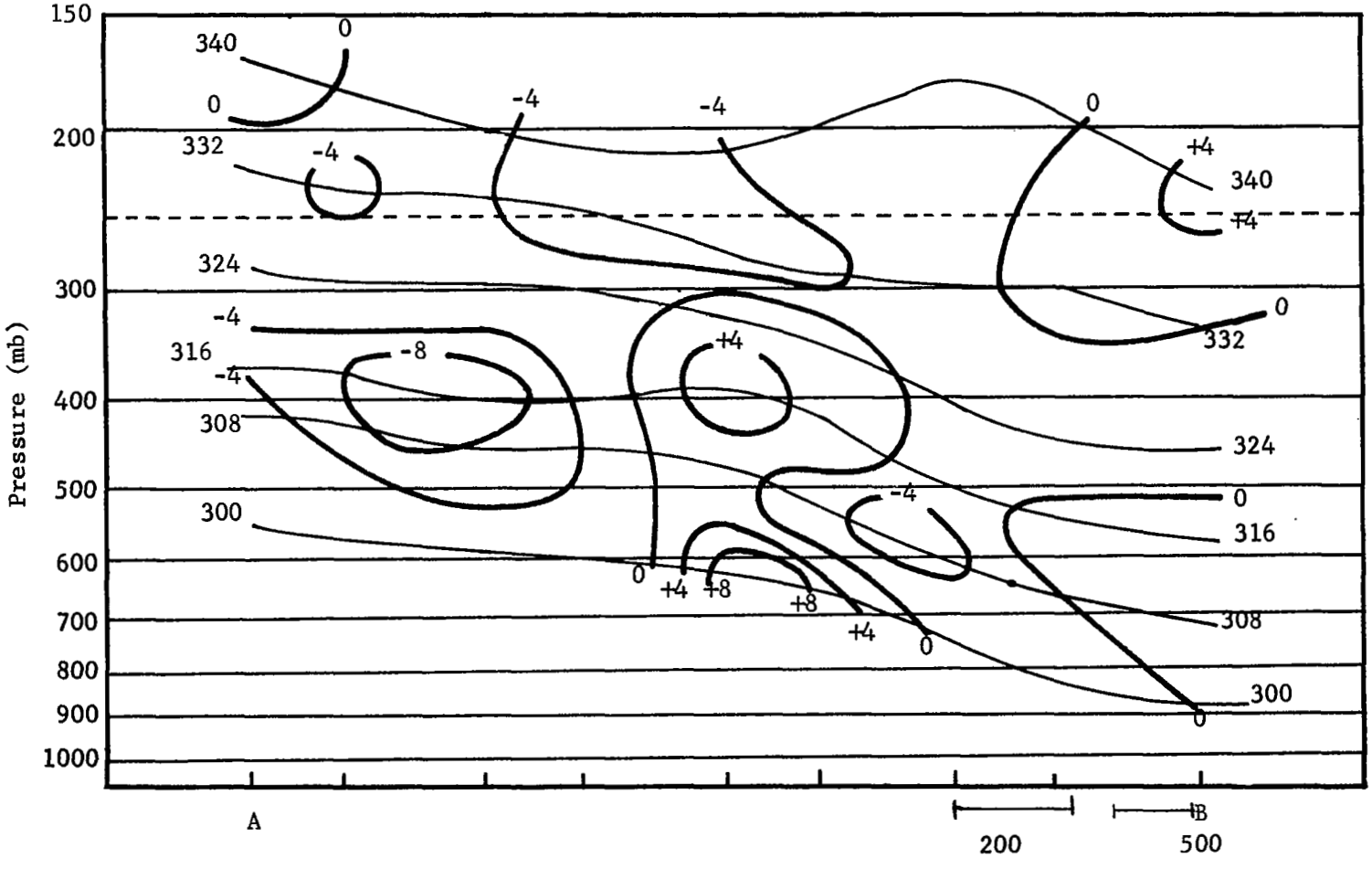

Fig. 19. Cross section along line AB in Fig. 12 (0900 GMT 12 May 1974). Constructed similarly to Fig. 14 except fronts and tropopauses are not shown.

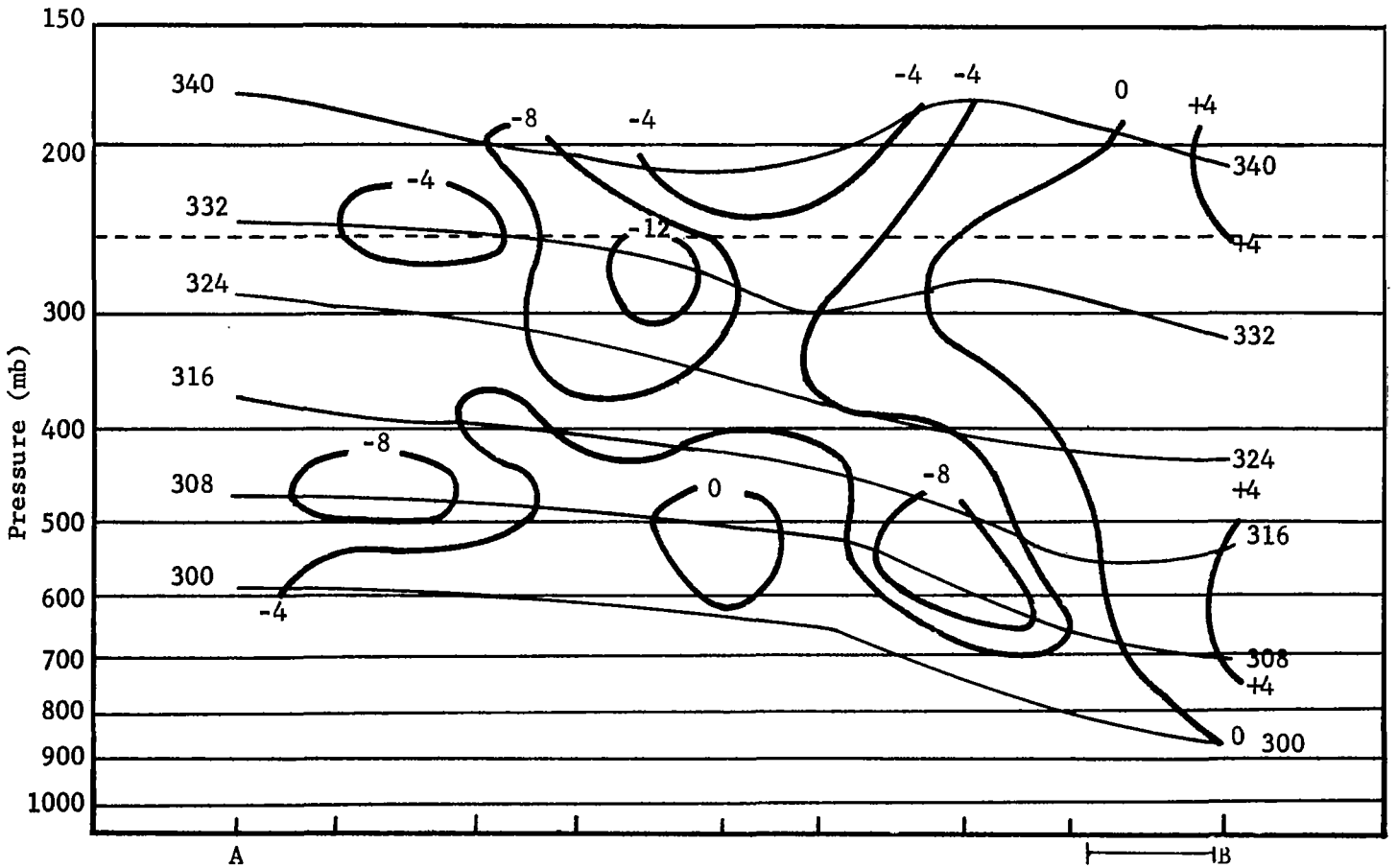

Fig. 20. Cross section along line AB in Fig. 13 (1200 GMT 12 May 1974). Constructed similarly to Fig. 14 except fronts and tropopauses are not shown.

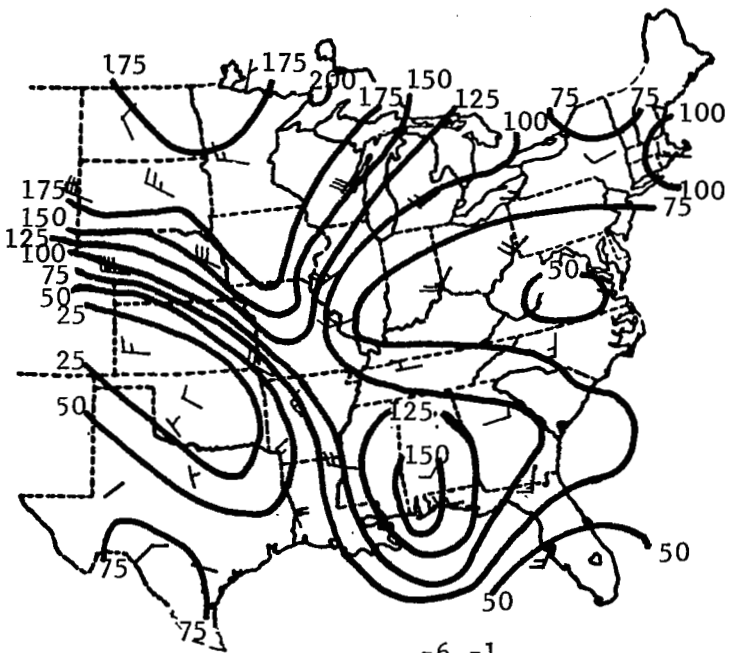

Fig. 21. Absolute vorticity (10^{-6} s^{-1}) on 308 K potential temperature surface for 0300 GMT, 12 May 1974. The units for wind are m s^{-1}.

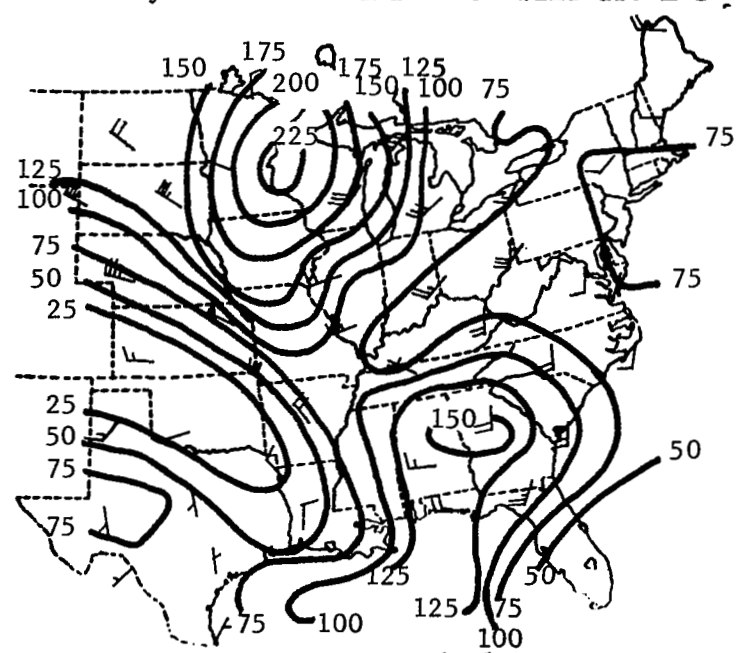

Fig. 22. Absolute vorticity (10^{-6} s^{-1}) on 308 K potential temperature surface for 0600 GMT, 12 May 1974. The units for wind are m s^{-1}.

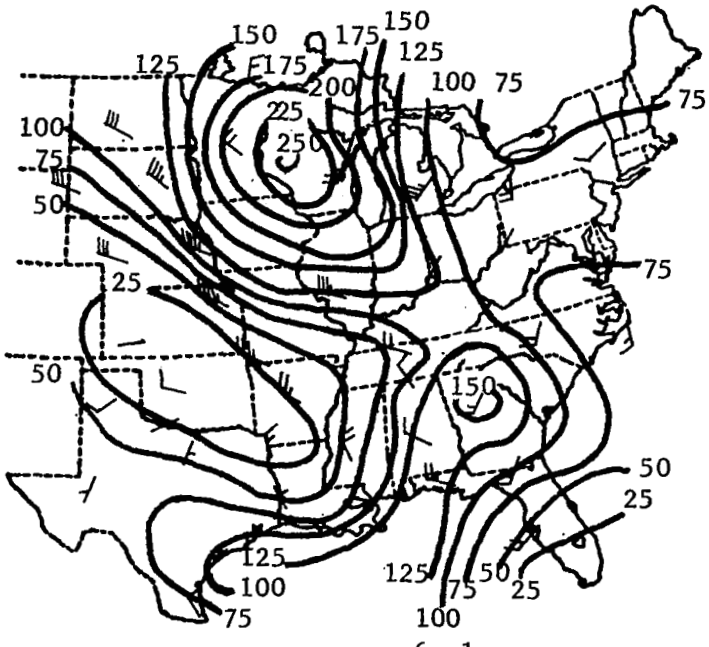

Fig. 23. Absolute vorticity (10^{-6} s^{-1}) on 308 K potential temperature surface for 0900 GMT, 12 May 1974. The units for wind are m s^{-1}.

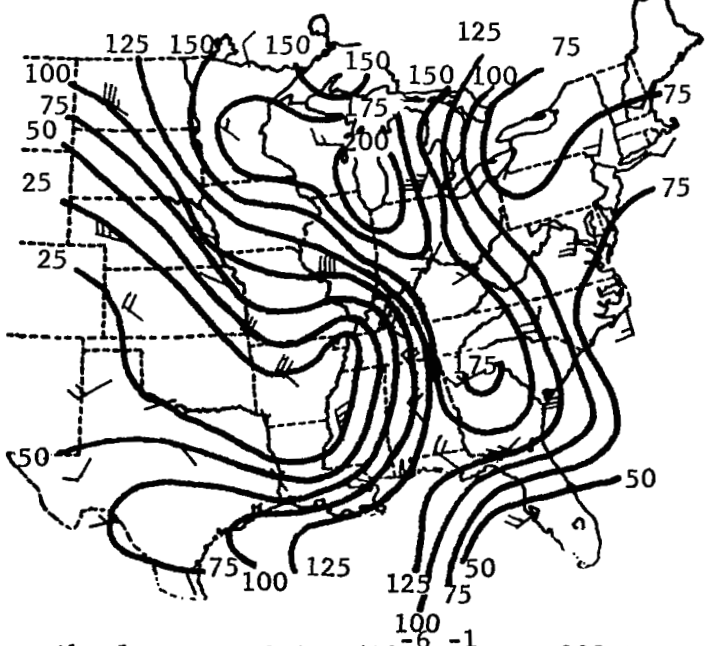

Fig. 24. Absolute vorticity (10^{-6} s^{-1}) on 308 K potential temperature surface for 1200 GMT, 12 May 1974. The units for wind are m s^{-1}.

respectively. When the fields of vertical motion are compared with the winds and vorticity, it is obvious that the waves in the wind field are related to the vertical motion fields. There is no geostrophic relation between wind and pressure gradient on isentropic charts, but in general the large-scale wind field tends to parallel the pressure contours. However, when perturbations in the wind field cause the streamlines to cross pressure contours, the last two terms in (2) contribute to vertical motion. The contribution made by these shortwave wind shifts to vertical motion is determined largely by their orientation to the slope of the isentropic surface.

Even though the most obvious shortwave patterns were associated with the frontal zone, they also were present in other areas. Upon inspection of the wind and vorticity charts, it can be seen that a shortwave wind shift moved around the east side of the cyclone located in the warm sector. Even though the magnitudes and gradients of vertical motion were less in this area than near the front, an area of upward motion developed southwest of Florida and moved to South Carolina during the last 6 h of the experiment.

Another feature of the wind field that is related directly to vertical motion is the axis of anticyclonically-curved flow that descends the dome of cold air. The axis of flow extended from southeast Nebraska to western Mississippi at 0300 GMT. By the end of the experiment, the axis had taken on a greater anticyclonic curvature and the wind speeds had increased. During the same period, a cell of downward motion was oriented along the axis with the downward motion

also increasing. As was pointed out in the last section, convection ended near the point where the vertical motion was downward over a deep layer. Now it can be seen that the convection stayed east of the anticyclonic axis of strong wind.

The identification of the stream just mentioned is possible because of the coordinate system used in this study, but the shortwave wind shifts mentioned previously can be identified by using standard pressure analysis. The identification of these shortwave phenomena can be made on many weather maps, but data taken at 12-h intervals do not provide enough information to permit these systems to be followed accurately in time. This analysis shows that such systems account for changes of vertical motion of as much as 20 cm s^{-1} within a horizontal distance of 300 km.

Some additional characteristics of the cross sections of vertical motion shown previously in Figs. 14 through 20 also are important in the interpretation of the motions. The vertical motions on each surface were calculated independently by using the method described in Section 4. Inspection of the cross sections shows that the method produced patterns that were coherent in the vertical and also reasonable according to current frontal models (Palmén and Newton, 1969). Frontal positions are indicated for the first two cross sections, but the cross sections intersect the upper front at an angle that makes frontal analysis of little use during the remaining time periods. The front at the latter times was becoming more diffuse and difficult to locate also

because of the interaction with the low-pressure system in the warm sector. Potential vorticity was used to aid in frontal and tropopause analysis. Large areas of negative vertical motion as pointed out by Danielsen (1968) were found in the stratosphere above the frontal zone.

Cells of vertical motion display continuity in time. The large positive value tends to stay in the area where the dome of cold air is sloping downward. In general, the motions are downward in the cold air and upward ahead of the front. Another interesting aspect of the vertical motion shown in the cross section is the vertical extent of the motions. Figure 18 shows that the depth of the short-wavelength area of vertical motion over Illinois (Fig. 11) was about 500 mb. The cross section in Fig. 19 passes through three of the short wave areas (Fig. 12) and shows all of them to be of comparable depth.

The location and depth of areas of vertical motion are significant in the maintenance of the identity of the cold dome. There was a large upward area associated with the pressure trough (troughs in pressure on isentropic surfaces indicate cold air) on the 308 K surface at 0600 GMT 12 May. Three hours later the trough in the pressure field was sharper, but by that time the areas of vertical motion associated with short waves had shifted so that downward motion was then moving into the area of the coldest air. By 1200 GMT 12 May most of the area covered by the cold air had downward motion at the 308 K level. Figure 20 shows a cross section along

line AB at 1200 GMT, from which it can be seen that the downward motions in the dome had great vertical extent. The collapse of the dome shows why the front was weakening rapidly by the end of the experiment.

b. Comparison of vertical velocity changes from 3- and 12-h rawinsonde data

While others (Scoggins et al., 1972; Bosart, 1969) have discussed vertical motion in their studies based on the AVE I data, no one has presented the vertical motion changes calculated by using 3-h data and compared them to the changes that would be calculated if only 12-h data were available. Kreitzberg and Brown (1970), Kreitzberg (1968), and Elliot and Hovind (1965) have shown the increased resolution from shorter intervals between measurements, but their studies were limited to small geographical areas. It is believed that the following charts which show changes of vertical motion over 3- and 12-h periods are unique in that they cover a large area.

The largest changes over a 12-h period are of the order of 2 cm s^{-1} h^{-1} while changes over 3-h periods show magnitudes as large as 8 cm s^{-1} h^{-1}. Figures 25 through 31 show local changes in vertical motion, $\partial w/\partial t$, over 3-h intervals, and Figs. 32 through 35 show the changes for 12-h intervals.

As would be expected, the greatest changes on the 3- and 12-h charts occurred along the frontal zone. Away from the frontal zone, the largest changes in 3-h periods usually were of the order of

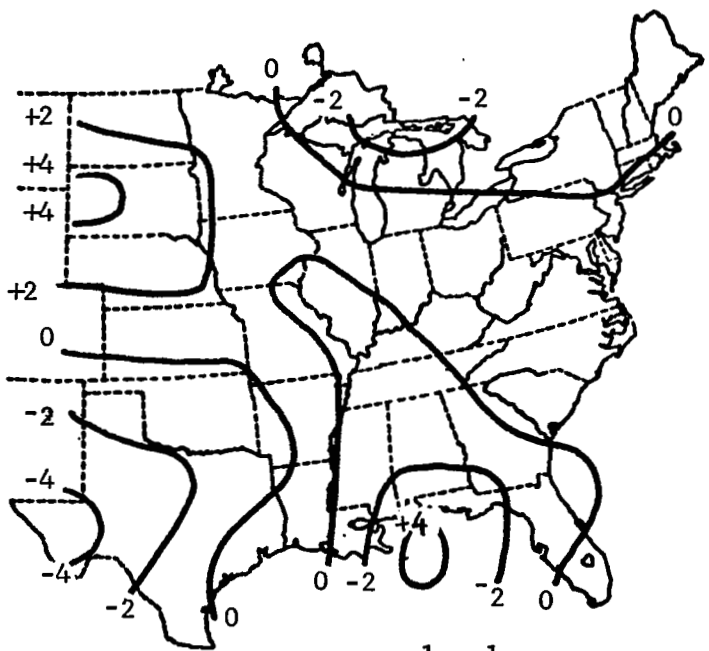

Fig. 25. Three-hour change (cm s^{-1} h^{-1}) in vertical motion on the 308 K potential temperature surface for the period ending at 1800 GMT 11 May 1974.

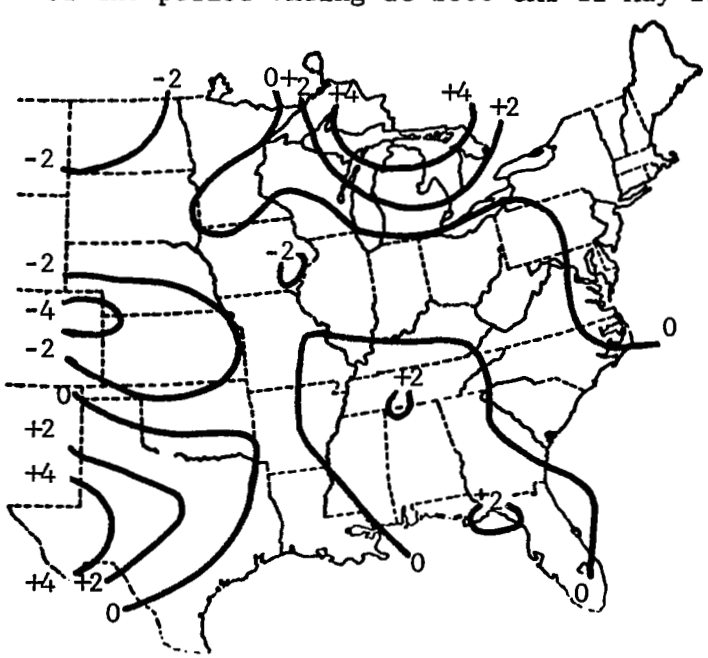

Fig. 26. Same as Fig. 25 except for period ending at 2100 GMT 11 May 1974.

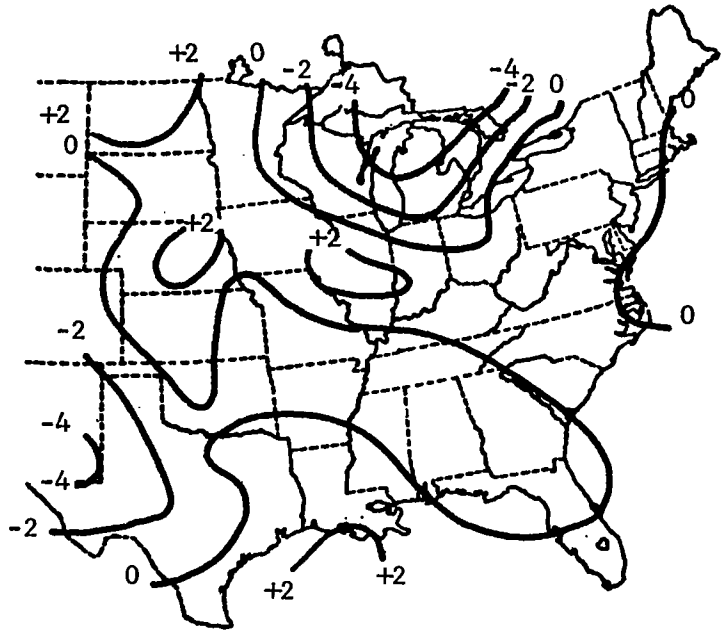

Fig. 27. Same as Fig. 25 except for period ending at 0000 GMT 12 May 1974.

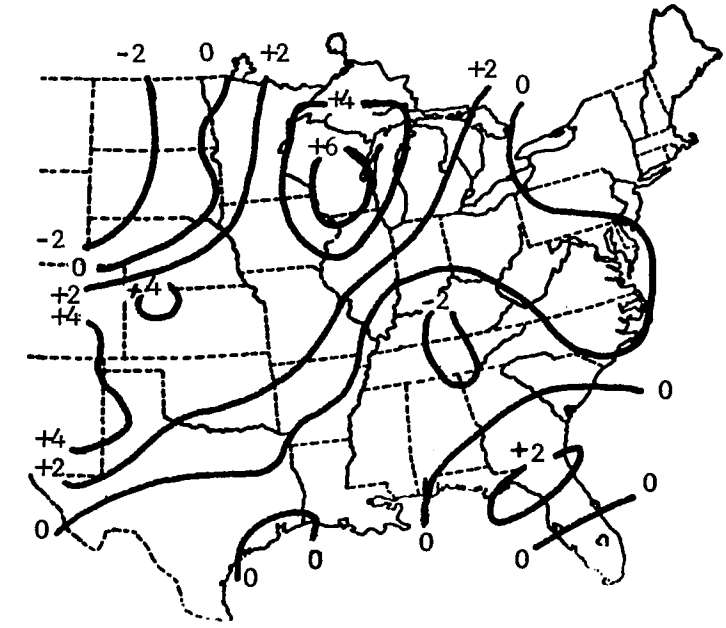

Fig. 28. Same as Fig. 25 except for period ending at 0300 GMT 12 May 1974.

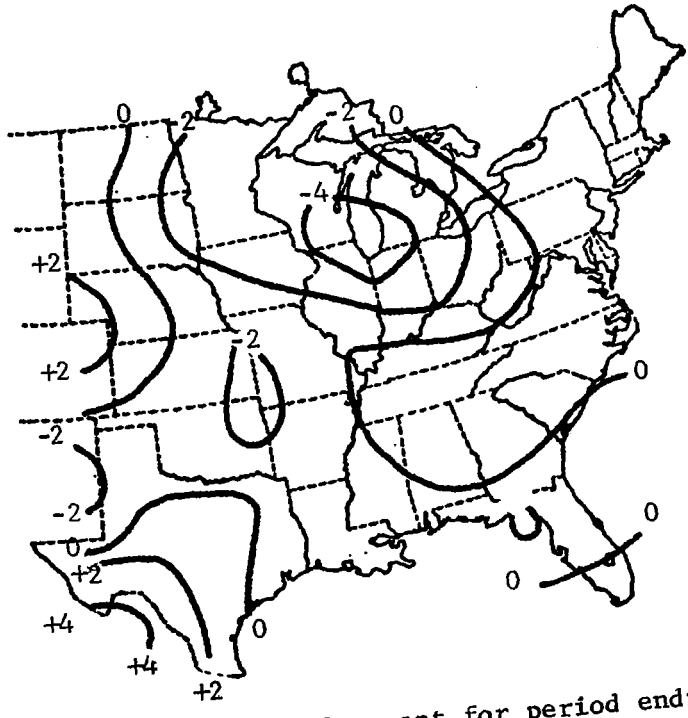

Fig. 29. Same as Fig. 25 except for period ending at 0600 GMT 12 May 1974.

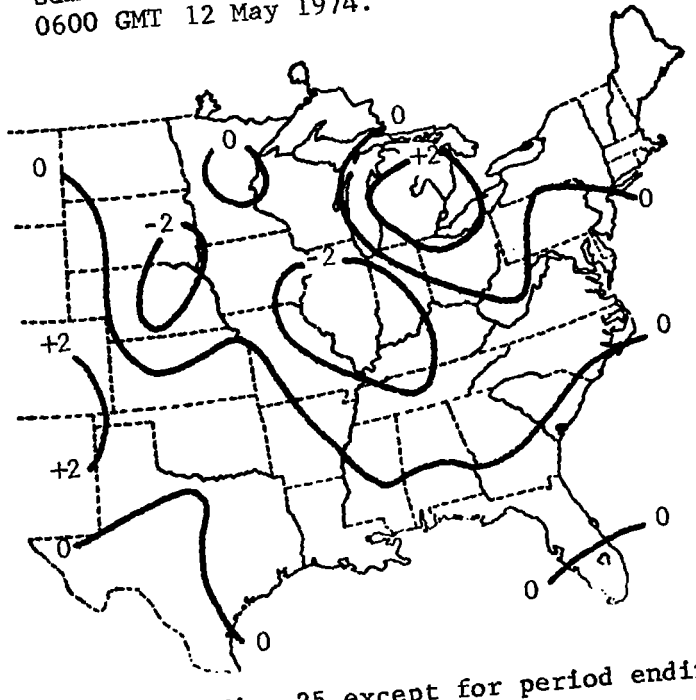

Fig. 30. Same as Fig. 25 except for period ending at 0900 GMT 12 May 1974.

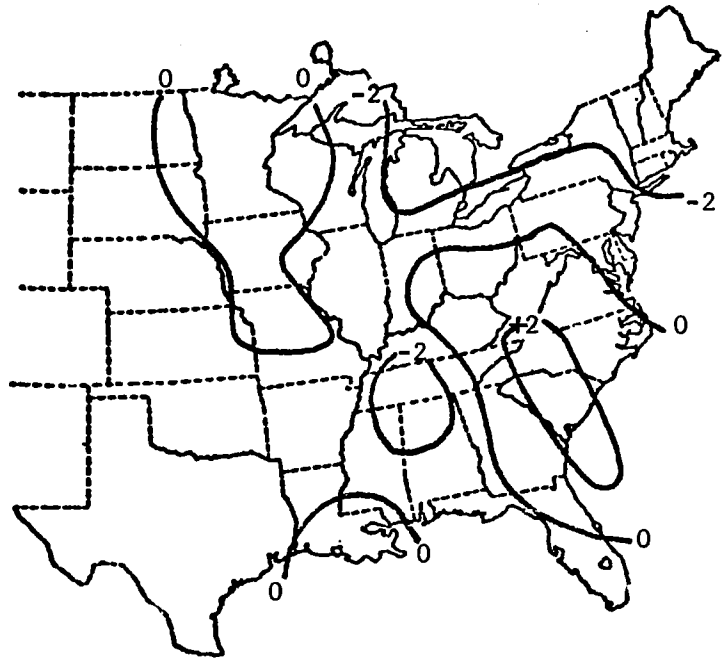

Fig. 31. Same as Fig. 25 except for period ending at 1200 GMT 12 May 1974.

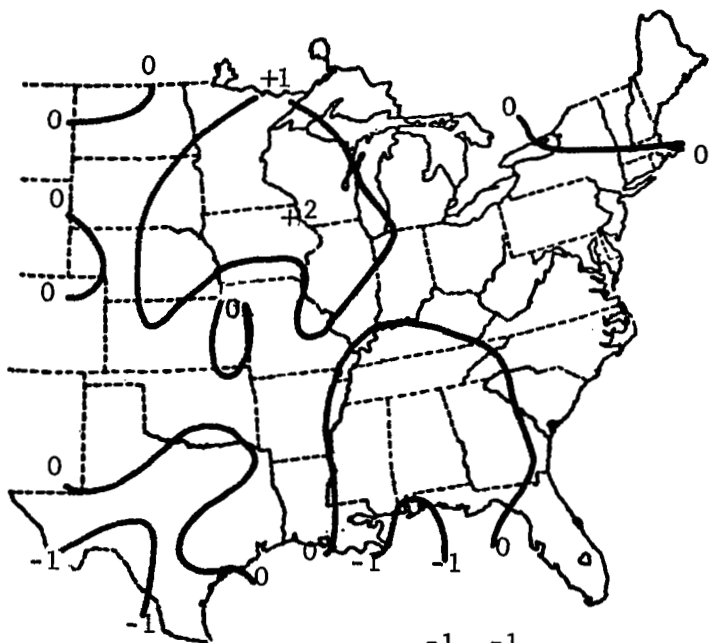

Fig. 32. Twelve-hour change (cm s^{-1} h^{-1}) in vertical motion on the 308 K potential temperature surface for the period ending at 0300 GMT 12 May 1974.

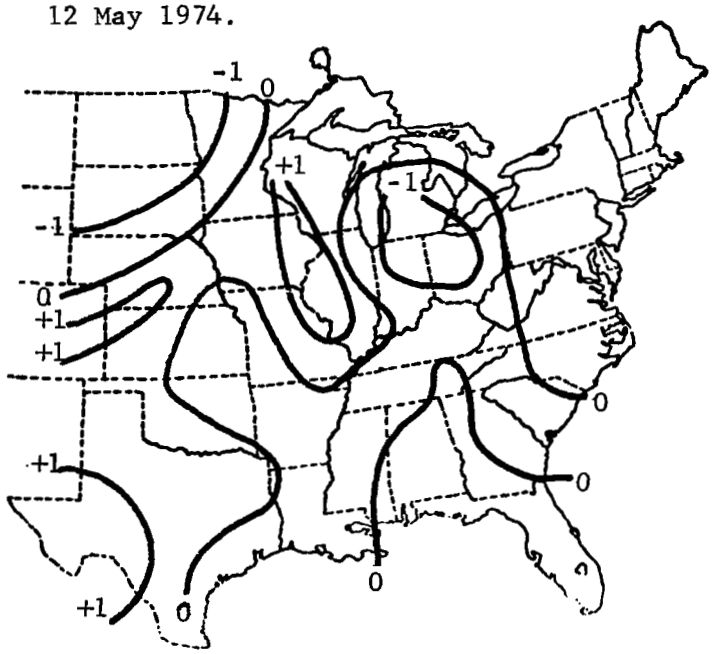

Fig. 33. Same as Fig. 32 except for the period ending at 0600 GMT 12 May 1974.

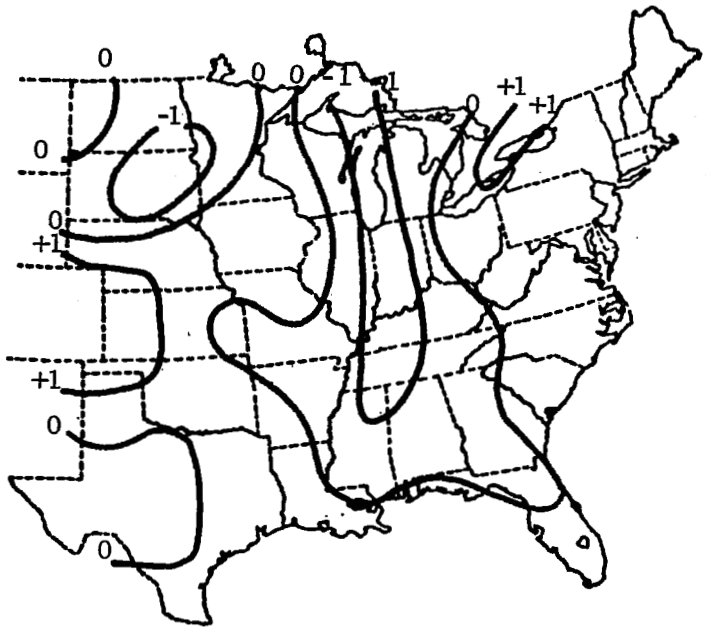

Fig. 34. Same as Fig. 32 except for the period ending at 0900 GMT 12 May 1974.

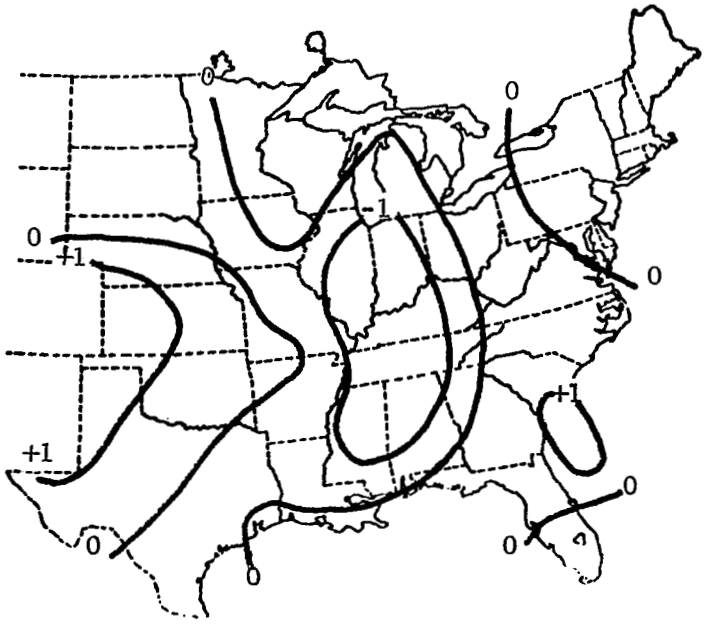

Fig. 35. Same as Fig. 32 except for the period ending at 1200 GMT 12 May 1974.

3 cm s^{-1} h^{-1}, while 2 cm s^{-1} h^{-1} was the largest change over 12 h calculated during the experiment. As an example of lost detail, the area of large increase centered over the Iowa-Wisconsin border for the 12-h period ending at 0300 GMT 12 May really reflects an increase that has taken place in the previous 3 h since there was little net change in the vertical motion in that area during the first 9 h of the period.

The rapid changes shown on the 3-h charts ending at 0600 GMT and 0900 GMT 12 May reflect the changes due to the shortwave systems discussed previously. Inspection of the 12-h change charts ending at the same times shows the great loss of detail due to the longer interval between measurements. The significant thing pointed out by these charts is the great increase in detail of the change in vertical motion when the interval of measurement is 3 h rather than 12 h. This greater time resolution may be of key importance in explaining and forecasting the occurrence of convective systems.

6. SUMMARY AND CONCLUSIONS

a. Summary

An objective analysis based on potential temperature as the vertical coordinate has been carried out. Analysis of pressure, absolute vorticity, vertical motion, and change of vertical motion has been accomplished on six potential temperature surfaces. The above analysis has been carried out on data that are unique in accuracy and sampling interval. The data were obtained under the auspices of the National Aeronautics and Space Administration during their AVE IIP project. Rawinsonde soundings at 54 sites were taken at 3-h intervals and great care was taken in the data reduction process. The analyzed fields have been used to study systems that are of a time scale that makes them impossible to follow from data taken at 12-h intervals.

b. Conclusions

This study has led to the following conclusions:

(1) Convection generally occurs in areas where the vertical motion is upward in the mid-troposphere;

(2) Convection generally does not penetrate into regions where the vertical motion is downward in excess of 4 cm s^{-1};

(3) Large-scale upward motion in the mid-troposphere does not necessarily imply that convection will occur;

(4) Mesoscale features (300-600 km) in the field of vertical

motion were observed in all areas, but their occurrence and intensity were greater near the cold front than in other areas in the synoptic situation studied;

(5) Near frontal zones, changes in vertical motion as great as 20 cm s^{-1} in a horizontal distance of 300 km were observed;

(6) Vertical motion changes calculated using 12-h rawinsonde data show maximum changes of 2 cm s^{-1} h^{-1} while 3-h data for the same period show changes as large as 8 cm s^{-1} h^{-1};

(7) Three-hour rawinsonde data greatly increase the number of small-scale features that can be followed in time;

(8) Rawinsonde data for every pressure contact greatly increases the accuracy of numerical calculations carried out from the data; and

(9) Rawinsonde soundings are required at 3-h intervals and possibly less in order to delineate areas of convection accurately; improvement of prediction should result from the improved delineation.

REFERENCES

Barnes, L., 1964: A technique for maximizing details in numerical weather analysis. J. Appl. Meteorol., 3, 396-409.

Barr, S., W. K. Widger, Jr., I. A. Miller, and R. Stanton, 1971: Objective subsynoptic upper level analysis. J. Appl. Meteorol., 10, 410-417

Bosart, Lance F., 1973: Detailed analyses of precipitation patterns associated with mesoscale features accompanying United States east coast cyclogenesis, Mon. Wea. Rev., 101, 1-12.

_____, 1969: Mid-tropospheric frontogenesis and potential vorticity behavior. Doctoral dissertation, Department of Meteorology, Massachusetts Institute of Technology, 132 pp.

Danielsen, E. F., 1968: Stratospheric-tropospheric exchange based on radioactivity, ozone and potential vorticity. J. Atmos. Sci., 25, 502-518.

Elliot, D., and E. L. Hovind, 1965: Heat, water, and vorticity balance in frontal zones. J. Appl. Meteorol., 4, 196-211.

Fuelberg, H. E., 1974: Reduction and error analysis of the AVE II Pilot experiment data, NASA Contractor Report CR-120496, NASA Marshall Space Flight Center, Huntsville, Alabama, 131 pp.

Kreitzberg, C. W., and H. A. Brown, 1970: Mesoscale weather systems within an occlusion. J. Appl. Meteorol., 9, 417-432.

_____, 1968: The mesoscale wind field in an occlusion. J. Appl. Meteorol., 7, 53-67.

Namias, J., 1940: An Introduction to the Study of Air Mass and Isentropic Analysis, 5th ed., Amer. Meteorol. Soc., 136-161.

Palmén, E., and C. W. Newton, 1969: Atmospheric Circulation Systems, Academic Press, New York, 237-370.

Petterssen, S., 1956: Weather Analysis and Forecasting Vol. I., McGraw-Hill, New York, 340-370.

Rossby, C. G. et al., 1937: Isentropic analysis. Bull. Amer. Meteor. Soc., 18, 201-209.

Saucier, W. J., 1955: Principles of Meteorological Analysis, The University of Chicago Press, Chicago and London, 250-261.

Scoggins, J. R., E. Wood, H. E. Fuelberg, and W. L. Reed, 1972: An investigaion of relationships between meso- and synoptic-scale phenomena, NASA Contractor Report, NASA CR-2030.

_____, H. E. Fuelberg, R. D. Carlson, R. W. Phelps, and D. G. Bellue, 1973: A compilation of studies from atmospheric variability experiment, NASA Contractor Report, NASA CR-2304.

APPENDIX I

Rawinsonde Stations Participating in AVE II Pilot Experiment

Station Identifier	Location
11001 (MSF)	Marshall Space Flight Center, Alabama
22001 (OUN)	Norman, Oklahoma
22002 (FSI)	Ft. Sill, Oklahoma
22003 (LNS)	Lindsay, Oklahoma
22004 (FTC)	Ft. Cobb, Oklahoma
22005 (CHK)	Chickasha, Oklahoma
201 (EYW)	Key West, Florida
202 (MIA)	Miami, Florida
208 (CHS)	Charleston, South Carolina
211 (TPA)	Tampa, Florida
213 (AYS)	Waycross, Georgia
221 (VPS)	Eglin AFB, Florida
226 (MGM)	Montgomery, Alabama
232 (BVE)	Boothville, Louisiana
235 (JAN)	Jackson, Mississippi
240 (LCH)	Lake Charles, Louisiana
248 (SHV)	Shreveport, Louisiana
250 (BRO)	Brownsville, Texas
255 (VCT)	Victoria, Texas
260 (SEP)	Stephenville, Texas
261 (DRT)	Del Rio, Texas
265 (MAF)	Midland, Texas
304 (HAT)	Hatteras, North Carolina
311 (AHN)	Athens, Georgia
317 (GSO)	Greensboro, North Carolina
327 (BNA)	Nashville, Tennessee
340 (LIT)	Little Rock, Arkansas
349 (UMN)	Monette, Missouri
363 (AMA)	Amarillo, Texas
402 (WAL)	Wallops Island, Virginia
405 (IAD)	Dulles Airport, Virginia
425 (HTS)	Huntington, West Virginia
429 (DAY)	Dayton, Ohio
433 (SLO)	Salem, Illinois
451 (DOC)	Dodge City, Kansas
456 (TOP)	Topeka, Kansas
486 (JFK)	Kennedy Airport, New York
494 (CHH)	Chatham, Massachusetts
518 (ALB)	Albany, New York
520 (PIT)	Pittsburgh, Pennsylvania
528 (BUF)	Buffalo, New York

APPENDIX I (Continued)

Rawinsonde Stations Participating in AVE II Pilot Experiment

Station Identifier	Location
532 (PIA)	Peoria, Illinois
553 (OMA)	Omaha, Nebraska
562 (LBF)	North Platte, Nebraska
606 (PWM)	Portland, Maine
637 (FNT)	Flint, Michigan
645 (GRB)	Green Bay, Wisconsin
654 (HUR)	Huron, South Dakota
655 (STC)	St. Cloud, Minnesota
662 (RAP)	Rapid City, South Dakota
712 (CAR)	Caribou, Maine
734 (SSM)	Sault Sainte Marie, Michigan
747 (INL)	International Falls, Minnesota
764 (BIS)	Bismarck, North Dakota

APPENDIX II

Standard heights of certain pressure levels

Pressure (mb)	Height (gpm)	Height (ft)
1000	111	364
900	988	3243
800	1949	6394
700	3012	9882
600	4206	13801
500	5574	18289
400	7185	23574
300	9164	30065
200	11784	38662

NASA-Langley, 1975